Clim Dyn
DOI 10.1007/s00382-013-1719-7

Regional and global projections of twenty-first century glacier mass changes in response to climate scenarios from global climate models

Valentina Radić · Andrew Bliss · A. Cody Beedlow · Regine Hock · Evan Miles · J. Graham Cogley

Received: 1 August 2012 / Accepted: 2 March 2013

Abstract A large component of present-day sea-level rise is due to the melt of glaciers other than the ice sheets. Recent projections of their contribution to global sea-level rise for the twenty-first century range between 70 and 180 mm, but bear significant uncertainty due to poor glacier inventory and lack of hypsometric data. Here, we aim to update the projections and improve quantification of their uncertainties by using a recently released global inventory containing outlines of almost every glacier in the world. We model volume change for each glacier in response to transient spatially-differentiated temperature and precipitation projections from 14 global climate models with two emission scenarios (RCP4.5 and RCP8.5) prepared for the Fifth Assessment Report of the Intergovernmental Panel on Climate Change. The multi-model mean suggests sea-level rise of 155 ± 41 mm (RCP4.5) and 216 ± 44 mm (RCP8.5) over the period 2006–2100, reducing the current global glacier volume by 29 or 41 %. The largest contributors to projected global volume loss are the glaciers in the Canadian and Russian Arctic, Alaska, and glaciers peripheral to the Antarctic and Greenland ice sheets. Although small contributors to global volume loss, glaciers in Central Europe, low-latitude South America, Caucasus, North Asia, and Western Canada and US are projected to lose more than 80 % of their volume by 2100. However, large uncertainties in the projections remain due to the choice of global climate model and emission scenario. With a series of sensitivity tests we quantify additional uncertainties due to the calibration of our model with sparsely observed glacier mass changes. This gives an upper bound for the uncertainty range of ±84 mm sea-level rise by 2100 for each projection.

Keywords Regional and global glacier mass changes · Projections of sea level rise · Global climate models

Electronic supplementary material The online version of this article (doi:10.1007/s00382-013-1719-7) contains supplementary material, which is available to authorized users.

V. Radić (✉) · E. Miles
Earth, Ocean and Atmospheric Sciences Department, University of British Columbia, 2020–2207 Main Mall, Vancouver, BC V6T 1Z4, Canada
e-mail: vradic@eos.ubc.ca

A. Bliss · A. C. Beedlow · R. Hock
Geophysical Institute, University of Alaska Fairbanks, 903 Koyukuk Dr., Fairbanks, AK 99775-7320, USA

E. Miles
Scott Polar Research Institute, University of Cambridge, Lensfield Road, Cambridge CB2 1ER, UK

J. G. Cogley
Department of Geography, Trent University, Peterborough, ON K9J 7B8, Canada

1 Introduction

Glaciers other than the ice sheets in Greenland and Antarctica (henceforth referred to as glaciers) are major contributors to sea-level rise (Hock et al. 2009; Kaser et al. 2006; Meier et al. 2007) but few studies have projected their mass changes and associated contribution to sea-level rise on a global scale (e.g., Raper and Braithwaite 2006; Marzeion et al. 2012; Slangen et al. 2012). Radić and Hock (2011) projected the volume changes of all glaciers until 2100, spatially resolved for 19 glacierized regions. More than 120,000 glaciers available in the extended World Glacier Inventory (Cogley 2009a) and covering 40 % of all global glacier area were modeled individually using

Published online: 02 April 2013

an elevation-dependent temperature-index mass-balance model. Future volume changes were then upscaled for each region with a scaling relation between the regional ice volume change and regional glacierized area. Projections were made in response to downscaled monthly temperature and precipitation scenarios of ten Global Climate Models (GCMs) based on the A1B emission scenario.

The purpose of this study is to update the projections by Radić and Hock (2011) aiming to improve quantification of the uncertainties. Since the publication of Radić and Hock (2011) a new global inventory has become available including nearly all glaciers in the world (Arendt et al. 2012) thus eliminating the uncertainty of upscaling. Also, new emission and climate scenarios have been released in preparation for the Fifth Assessment Report of the Intergovernmental Panel of Climate Change (IPCC AR5). Here we use simulations from 14 GCMs under two of the most recent emission scenarios to drive transient simulations of glacier volume change for 19 regions. As in Radić and Hock (2011), we consider the climatic mass balance (the sum of surface and internal mass balance; Cogley et al. 2011) but neglect mass losses by calving or subaqueous melting.

The paper is organized as follows: in Sect. 2 we describe the input data needed for running our glacier mass balance model on global scale. Section 3 briefly explains the model setup and calibration, focusing on the differences from the model setup in Radić and Hock (2011). This section also includes model validation using all available in situ mass balance observations. The projected regional and global glacier volume losses are presented and discussed in Sect. 4, including the analysis of regional mass balance sensitivities. Finally, in Sect. 5 we quantify uncertainties in the projections by using a series of sensitivity tests and an error analysis, and present the conclusions in Sect. 6.

2 Data

2.1 Glacier inventory and initial volumes

Here we use the Randolph Glacier Inventory Version 2 (hereafter "RGI"; Arendt et al. 2012), which is the first dataset containing outlines of almost all glaciers in the world. The inventory is a recent community effort that combines glacier outlines from the Global Land Ice Measurements from Space (GLIMS) initiative with other glacier outlines assembled from a variety of existing databases, as well as new outlines provided by various contributors. The inventory includes the peripheral glaciers in Antarctica (Bliss et al. 2013) and Greenland (Rastner et al. 2012). The inventory is divided into 19 regions (Fig. 1), following Radić and Hock (2010) with only minor modifications, and 56 subregions.

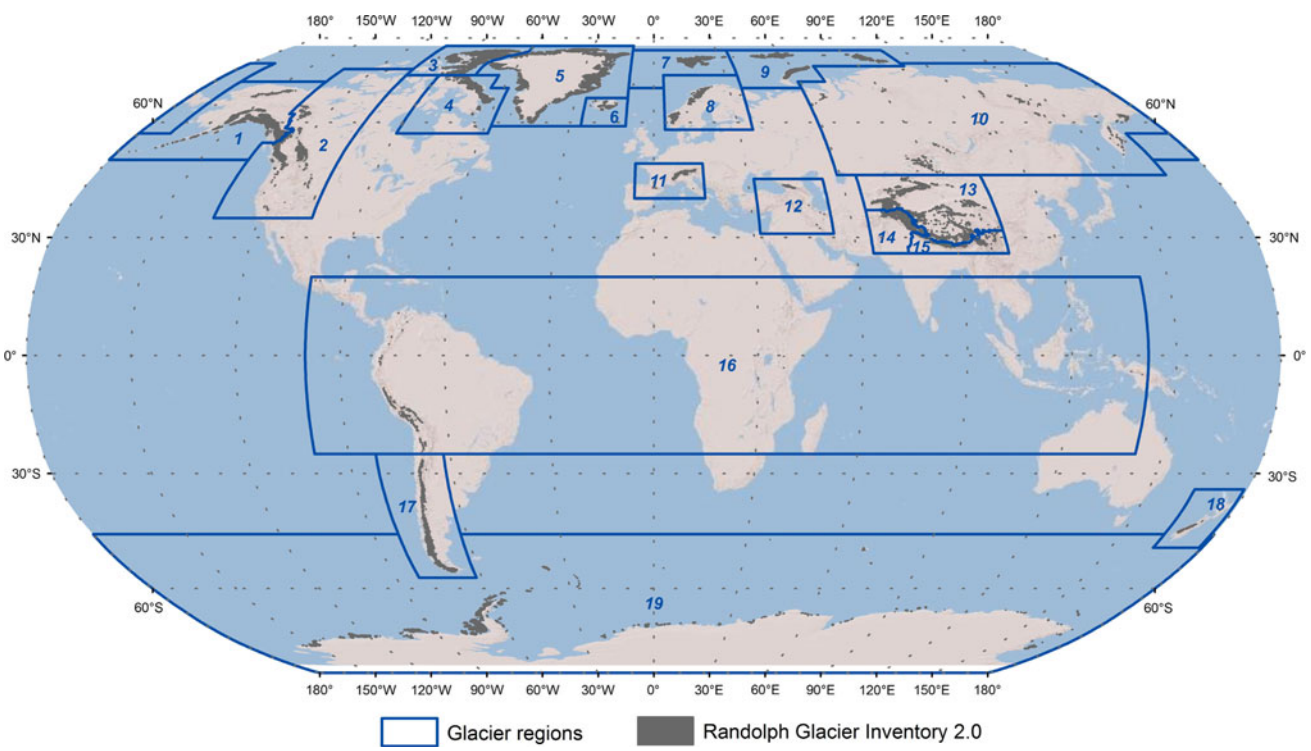

Fig. 1 Location of global glaciers divided into *19 regions*. Data is from the Randolph Glacier Inventory 2.0 (Arendt et al. 2012)

In most regions, the outlines in Randolph Glacier Inventory represent glaciers, however in some regions (see Supplementary Table S1) some of the outlines represent glacier complexes (collections of glaciers that meet at ice divides). For these complexes we delineated individual glaciers with an automated tool (C. Kienholz, personal communication). The RGI does not differentiate between mountain glaciers and ice caps. Therefore, we assume that all RGI glaciers are mountain glaciers, except in Iceland where glaciers and ice complexes are considered as ice caps. For Antarctic and Subantarctic region we differentiate between ice caps and mountain glaciers following Bliss et al. (2013). In total the delineated RGI inventory consists of 200,295 glaciers covering an area of 736,989 km^2 (Table 1).

The area of each individual glacier is needed since volume-area scaling is applied to estimate the initial ice volume, and the relation between volume and area is not linear. A power law relationship between volume and area was originally derived from measurements (Chen and Ohmura 1990). The theoretical basis for this relationship is explained in Bahr et al. (1997) using scaling analysis for glaciers in a steady state. Following Radić and Hock (2010) we compute the volume, V, of each glacier from its area, S, according to

$$V = cS^{\gamma} \quad (1)$$

assuming scaling coefficients for mountain glaciers ($c = 0.2055$ m$^{3-2\gamma}$, $\gamma = 1.375$) and ice caps ($c = 1.7026$ m$^{3-2\gamma}$, $\gamma = 1.25$). Estimates of glacierized area, number of glaciers and initial volumes for each of 19 regions are provided in Table 1.

2.2 Glacier hypsometry

For each glacier we derive glacier hypsometry using available digital elevation models (DEMs). For most regions between 60°N and 60°S we used the hole-filled Version 4 Shuttle Radar Topographic Mission (SRTM) DEM with a resolution of about 90 m (Jarvis et al. 2008). For the following regions we used DEMs from other sources: for the Canadian Arctic a DEM assembled from 149 Canadian Digital Elevation Data (CDED) tiles, for the Russian Arctic a DEM assembled from GLAS/ICESat L2 data (Zwally et al. 2012), for Greenland the Greenland Mapping Project (GIMP) Digital Elevation Model (Version

Table 1 Basic inventory statistics for each region

#	Region	N	S (km^2)	V (km^3)	SLE (mm)	S_0 (km^2)	N ($S > S_0$)	N ($S < S_0$)	V* (km^3)	SLE* (mm)
1	Alaska	26,190	89,051	27,868	69.3	100	136	26,054	18,595	46.2
2	Western Canada and US	14,042	14,505	1,275	3.2	10	162	13,880	1,275	3.2
3	Arctic Canada (North)	3,330	105,002	55,545	138.1	1000	16	3,314	34,716	86.3
4	Arctic Canada (South)	7,319	40,885	9,356	23.3	100	53	7,266	6,994	17.4
5	Greenland	21,943	87,810	17,130	42.6	100	108	21,835	13,588	33.8
6	Iceland	545	11,058	2,655	6.6	100	22	523	2,655	6.6
7	Svalbard	1,560	33,837	9,089	22.6	100	82	1,478	6,799	16.9
8	Scandinavia	2,318	2,852	201	0.5	10	52	2,266	202	0.5
9	Russian Arctic	963	51,784	17,778	44.2	100	103	860	12,240	30.4
10	North Asia	3,236	2,820	274	0.7	10	39	3,197	274	0.7
11	Central Europe	6,622	2,061	139	0.3	10	27	6,595	139	0.3
12	Caucasus and Middle East	1,298	1,100	68	0.2	10	16	1,282	68	0.2
13	Central Asia	45,513	67,970	6,480	16.1	100	32	45,481	6,072	15.1
14	South Asia (West)	23,051	33,859	4,475	11.1	100	33	23,018	3,792	9.4
15	South Asia (East)	14,116	21,775	1,852	4.6	100	7	14,109	1,803	4.5
16	Low Latitudes	4,373	4,040	231	0.6	10	30	4,343	231	0.6
17	Southern Andes	17,438	32,547	6,842	17	100	43	17,395	5,118	12.7
18	New Zealand	3,686	1,165	79	0.2	10	17	3,669	79	0.2
19	Antarctic and Subantarctic	2,752	132,867	48,636	120.9	1000	36	2,716	48,636	120.9
	Global	200,295	736,989	209,973	522.0				163,277	405.9

N total number of glaciers, *S* glacierized area, *V* ice volume derived from volume-area scaling, *SLE* volume in sea-level equivalent (assuming ice density of 900 kg m^{-3} and ocean area of 362 $\times$ 10^{12} m^2), S_o (see text) threshold glacier area to distinguish large and small glaciers, $N(S > S_o)$ number of large glaciers, $N(S \leq S_o)$ number of small glaciers, *V** alternative estimate for total ice volume (assuming that all glaciers with area $> S_o$ for Arctic regions, High Mountain regions and Southern Andes are ice caps), *SLE** total alternative volume in sea level equivalent

1.0 available at http://bprc.osu.edu/GDG/gimpdem.php), for New Zealand the NZSoSDEM v1.0 DEM produced at University of Otago (Columbus et al. 2011) resampled to 90 m, and for Alaska the National Elevation Dataset (NED) DEM maintained by US Geological Survey. For the remaining regions north of 60° we used the Advanced Space-borne Thermal Emission and Reflection Radiometer (ASTER) GDEM version 2 (Tachikawa et al. 2011). For the Antarctic and Subantarctic region we used the Radarsat Antarctic Mapping Project DEM (RAMP; Liu et al. 2001) supplemented by SRTM and GDEM2. A summary of the applied DEMs including their original resolution is given in Supplementary Table S1. Glacier hypsometries are created for 20 m elevation bands for all the regions except Alaska, where 25 m elevation bands were used.

2.3 Mass balance data

We calibrate the glacier mass balance model (Sect. 3.2) using regional mass balance estimates for 56 RGI subregions (listed in Supplementary Table S2). The regional estimates were interpolated on a pentadal (5-yearly) basis for 1961–2010 from an updated database of mass-balance measurements using the methods of Cogley (2009b; hereafter "C09") and regional glacierized areas from the RGI. For the purpose of this analysis, mass-balance data from tidewater glaciers were excluded; hence the regional estimates only refer to climatic mass balance to allow direct comparison with the results from our model. There were almost 4,000 directly measured annual mass budgets from more than 300 glaciers, and more than 15,000 annual values from multi-annual volume change measurements from an additional >250 glaciers.

For validation of our modeled mass changes for present-day climate we use seasonal direct mass balance observations from 137 glaciers (Dyurgerov 2010). The overlap between this and C09 dataset is discussed in Sect. 3.2.

2.4 Climate data

For consistency with the data used in Radić and Hock (2011), climate forcing for the calibration period (1961–2000) is from climate reanalysis and gridded climatology products. The model is forced with monthly mean near-surface air temperature and precipitation. For temperature we use the ERA-40 reanalysis of the European Centre for Medium Range Weather Forecasts (ECMWF; Kållberg et al. 2004), which is derived for the period from mid-1957 to mid-2002 and covers the whole globe with spectral resolution TL159, corresponding to a grid-spacing close to 125 km (1.125°). We extract 6-hourly 2 m air temperature reanalyses onto a bi-linearly interpolated grid with 0.5° × 0.5° resolution and compiled them into monthly means. For precipitation we use a climatology prepared by Beck et al. (2005) which provides monthly globally 0.5° × 0.5° gridded data of all available measured precipitation on land for the period 1951–2000. We chose the climatology rather than ERA-40 reanalysis because the precipitation reanalysis often needs further downscaling, especially for the high elevation sites, which are common sites for glaciers. The climatology is prepared at the Global Precipitation Climatology Centre in the frame of the project VASClimO which is part of the German Climate Research Programme (DEKLIM). We extract monthly precipitation sums from January 1961 to December 2000 interpolated to a 0.5° × 0.5° grid. All the missing values in VASClimO (which were fewer than 1 % of the total data points used) are replaced with ERA-40 precipitation.

For the projections of glacier volume change we use time series of monthly 2 m air temperature and precipitation from 14 GCMs selected from Coupled Model Intercomparison Project Phase 5 (CMIP5) models (Table 2; Taylor et al. 2012). For the CMIP5, a series of modeling studies conducted for the IPCC AR5 assessment, four new emission scenarios were developed and are referred to as Representative Concentration Pathways (RCP2.6, RCP4.5, RCP6.0, and RCP8.5). The RCPs are mitigation scenarios, based on a range of projections of future population growth, technological development, and societal responses, which assume that policy actions will be taken to achieve certain emission targets (Moss 2010). We select the two scenarios RCP4.5 and RCP8.5 for our modeling of future glacier mass changes. The labels for the RCPs provide a rough estimate of the radiative forcing in the year 2100 relative to preindustrial conditions. RCP8.5, which can be referred to as a "high-emission scenario", has a radiative forcing that increases throughout the twenty-first century before reaching a level of about 8.5 Wm^{-2} at the end of the century. The intermediate scenario RCP4.5 reaches a level of about 4.5 Wm^{-2} by the end of the twenty-first century.

3 Methods

A brief summary of our method is as follows: First, we run the elevation-dependent mass-balance model by Radić and Hock (2011) for each individual glacier for the period 1961–2000 forced by monthly mean temperature and precipitation. Most model parameters are taken from Radić and Hock (2011) but some are recalibrated using updated regional mass-balance datasets available in this study (i.e. estimates of area-averaged mass balance on a regional scale). In this way we obtain initial regional and global mass balances prior to projections. The calibrated and initialized model is then validated against in situ observations of climatic mass balance for individual glaciers.

Table 2 Characteristics of the 14 GCMs used in this study

Model name	Modeling center	Country of origin	Surface resolution (°)
BCC-CSM1.1	Beijing Climate Center China Meteorological Administration	China	2.8125 × 2.8125
CanESM2	Canadian Centre for Climate Modeling and Analysis	Canada	2.8125 × 2.8125
CCSM4	National Center for Atmospheric Research	United States	0.9 × 1.25
CNRM-CM5	Centre National de Recherches Meteorologiques/Centre Europeen de Recherche et Formation Avancees en Calcul Scientifique	France	1.40625 × 1.40625
CSIRO-Mk3-6-0	Commonwealth Scientific and Industrial Research Organization in collaboration with Queensland Climate Change Centre of Excellence	Australia	1.875 × 1.875
GFDL-CM3	NASA Geophysical Fluid Dynamics Laboratory	United States	2 × 2.5
GISS-E2-R	NASA Goddard Institute for Space Studies	United States	2 × 2.5
HadGEM2-ES	Met Office Hadley Centre	United Kingdom	1.24 × 1.875
INM-CM4	Institute for Numerical Mathematics	Russia	1.5 × 2
IPSL-CM5A-LR	Institut Pierre-Simon Laplace	France	1.9 × 3.75
MIROC-ESM	Japan Agency for Marine-Earth Science and Technology, Atmosphere and Ocean Research Institute (The University of Tokyo) and National Institute for Environmental Studies	Japan	2.8125 × 2.8125
MPI-ESM-LR	Max Planck Institute for Meteorology	Germany	1.875 × 1.875
MRI-CGCM3	Meteorological Research Institute	Japan	1.125 × 1.125
NorESM1-M	Norwegian Climate Centre	Norway	1.875 × 1.875

Finally, we run the calibrated mass balance model for all RGI with downscaled monthly twenty-first century temperature and precipitation from 14 GCMs, based on the two chosen emission scenarios (RCP4.5 and RCP8.5). We use volume-length scaling to account for the feedback between glacier mass balance and changes in glacier hypsometry, allowing receding glaciers to approach a new equilibrium in a warming climate.

3.1 Mass balance model

We calculate the specific climatic mass balance for each elevation band of a glacier as a sum of accumulation, ablation and refreezing. Ablation, a (mm water equivalent, w.e.) is calculated through a temperature-index model as

$$a = f_{ice/snow} \int \max(T, 0) dt \tag{2}$$

where $f_{ice/snow}$ is a degree-day factor for ice or snow (mm w.e. day^{-1} °C^{-1}), and T is surface air temperature (°C). The degree-day factor for snow, f_{snow}, is used above an assumed elevation of the firn line (i.e. the line separating firn from bare ice at the end of the melt season) regardless of snow cover, while below the elevation of the firn line we apply f_{ice} when snow depth is zero and f_{snow}, when snow depth is greater than zero. The firn line elevation is set to the mean glacier altitude. For the calibration period (1961–2000) glacier area and hypsometry are kept constant in time, so the firn line elevation is also constant. For the future projections it is time dependent since the glacier elevation range can change according to the scaling relation between glacier area and length (see Sect. 3.4). Monthly snow accumulation, C (mm w.e.), is calculated for each elevation band as

$$C = \delta_m P_m \begin{cases} \delta_m = 1, & T_m < T_{snow} \\ \delta_m = 0, & T_m \geq T_{snow} \end{cases} \tag{3}$$

where P_m is monthly precipitation (mm) which is assumed to be snow if the monthly temperature T_m (°C) is below the threshold temperature, T_{snow}, which discriminates snow from rain precipitation. Potential depth of annual refreezing is empirically related to the annual mean air temperature following Woodward et al. (1997). Any snow that melts from a given elevation band refreezes at depth in the

snow pack until the potential depth has been met, after which additional melt runs off the glacier.

To correct for the bias of the reanalysis temperature with respect to the local temperature on a glacier we apply a statistical lapse rate, lr_{ERA}, to estimate the temperature at the top of the glacier from that at the ERA-40 altitude of the grid cell containing the glacier. Then from the glacier top to the snout of the glacier we apply another lapse rate, lr, to simulate the increase in temperature as elevation decreases along the glacier surface. The bias in precipitation is corrected by assigning a precipitation correction factor, k_P, to estimate precipitation at the glacier top. To account for orographic effect we distribute the precipitation from the top to the snout of the glacier using a precipitation gradient d_{prec} (% of precipitation decrease per meter of elevation decrease).

Winter mass balance and summer mass balance are integrated over the winter and summer season, respectively. The beginning of winter (summer) for glaciers located in the northern hemisphere north of 75°N is 1 September (1 May) otherwise it is 1 October (1 April), while for glaciers in the southern hemisphere it is 1 April (1 Oct). The model is described in further detail in Radić and Hock (2011; supplementary material).

3.2 Calibration and initialization of the mass balance model

We follow a similar calibration method as in Radić and Hock (2011), and here only provide a brief summary. Radić and Hock (2011) applied the model to 36 glaciers world-wide and used time series of observed area-averaged winter and summer mass balance, and seasonal mass balance profiles, for deriving the values of seven model parameters (lr_{ERA}, lr, f_{snow}, f_{ice}, k_P, d_{prec} and T_{snow}) for each of these glaciers. In order to assign parameter values to all the glaciers in the world they used a set of empirical functions, which relate some of the model parameters (f_{snow}, f_{ice}, k_P) to the climatic setting of each glacier defined by a continentality index (range of the annual cycle of temperature) and annual sum of precipitation, both assessed from the climate datasets (ERA-40 for temperature, and VASClimo for precipitation) and averaged over the 20-year period 1980–1999. For three of the remaining four parameters (lr, d_{prec} and k_P) that could not be related to climate setting they assumed that the mean value from the sample of 36 glaciers is a good first-order approximation for all glaciers.

Here we adopt the values of Radić and Hock (2011) for these model parameters, and model the mass-balance of all glaciers for our calibration period 1961–2000. Sensitivity experiments in Radić and Hock (2011) showed that the model is particularly sensitive to the choice of the parameter lr_{ERA} because of the dominant role of temperature in controlling glacier mass balance. Therefore we retune lr_{ERA} for each of the 56 subregions by minimizing the root-mean-square error between modeled and C09 estimated pentadal area-averaged mass balances over 1961–2000. The tuning is performed for all the regions except Antarctic and Subantarctic where the value for lr_{ERA} is adopted from Radić and Hock (2011). This retuning procedure is justified since our aim is not to hindcast regional mass balances but rather to obtain initial balances for our future projections. Initializing the mass balance on the regional scale allows for significant discrepancies in modeled mass balance at the scale of individual glaciers. To reduce these discrepancies, especially for large glaciers which carry most of the weight in the area-average mean, we separate "large" from "small" glaciers for each of the 19 regions and perform the tuning independently for each sample. The separation is done at a threshold area of 10, 100 or 1,000 km^2 (Table 1) depending on the region. This segregated initialization reduced but did not eliminate the occurrence of unrealistic balances for individual glaciers. For example, some glaciers had no modeled melt in any year, while some gained modeled mass over the ablation season throughout the calibration period. To correct for this behaviour we perform final tuning by identifying poorly simulated glaciers in each region as outliers and re-tuning the parameter lr_{ERA} for a regional sample consisting only of the outliers. The number of outliers for each region is given in Supplementary Table S3, including the reason why they are identified as outliers. The final values of the tuned parameters for each subregion are presented in Supplementary Table S2.

3.3 Validation of the mass balance model

When the initialized and calibrated model is run for each glacier over the period 1961–2000 we derive a global mass balance of −0.34 m w.e. year^{-1}, which agrees well with previous estimates (e.g., Dyurgerov and Meier 2005; Kaser et al. 2006). In Fig. 2 we present the annual, winter and summer mass balance area-averaged over all glaciers for the period 1961–2000, as well as the C09 estimates of global pentadal mass balance which were used for model initialization. As shown in Fig. 2 for the pentadal mass balance time series, there are still some differences between C09 mass balance estimates and our modeled balances. This is expected, since the model initialization is performed by minimizing the root-mean-square error between the modeled and estimated pentadal series, meaning that an exact match has not been aimed for. We keep in mind that C09 estimates are derived from extrapolation/interpolation from all available mass balance observations, which represent fewer than 1 % of glaciers worldwide, while we model the mass balance for every

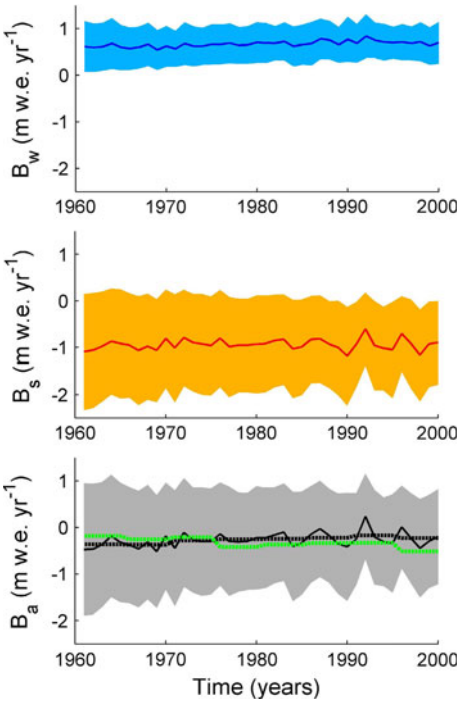

Fig. 2 Time series of modeled winter (B_w), summer (B_s) and annual (B_a) mass balance area-averaged over all glaciers for 1961–2000. The *shaded area* represents one spatial standard deviation for each year. Pentadal averages of modeled annual balances (*black dashed line*) are shown for comparison with the estimated pentadal annual balances (*green line*) from an updated version of Cogley (2009b)

glacier in the world. Although C09 estimates represent the most detailed assessment of the past mass-balance time series on regional and global scale, they are vulnerable to under-sampling and are therefore highly uncertain. In Sect. 4.4.1 we address how these uncertainties in model initialization impact our projections of regional and global volume loss.

To test the validity of our modeling approach in simulating individual glacier mass balances we use seasonal specific mass balance data from 137 glaciers, compiled in Dyurgerov (2010). The majority of these glaciers are incorporated in the C09 estimates of regional mass balance and therefore our model validation is not completely independent from the model calibration. However, C09 used only multi-annual and annual mass balance observations, while we validate winter and summer mass balances independently. Also, our model calibration is performed by minimizing the misfit between modeled and C09 estimated regional mass balances while, in the validation, we look at the model performance for individual glaciers with in situ mass balance observations. In other words, the calibration is taking into account the mean of a large sample, while the validation is focused on the individual members of the sample.

The number of in situ seasonal mass balance observations compiled in Dyurgerov et al. (2010) is inhomogeneous worldwide, with most measurements in Scandinavia (44 glaciers) and Western Canada and US (27 glaciers), while some regions (Arctic Canada South, South Asia West and East, Low Latitudes, Antarctic and Subantarctic) have no observations at all within the period 1961–2000. In Fig. 3 we compare modeled and observed seasonal mass balances regions containing observations within the validation period. The modeled mass balances are derived for the RGI glacier that corresponds (i.e. is the exact match) to a selected observed glacier in each region. For most sites the RGI glacier needed to be identified manually, while in a few cases where the exact match could not be found the spatially closest RGI glacier to the observed one is identified as the match. The results of the validation are summarized in Table 3: in terms of root-mean-square-error (RMSE), bias (difference between the modeled and observed specific mass balance averaged over the glacier sample), and correlation between modeled and observed specific mass balances for each region. For the biases and the correlation coefficients we also provide a statistical test of significance (Table 3). RMSE averaged over the 14 regions is 0.9 $\pm$ 0.5 and 1.1 $\pm$ 0.5 m w.e year^{-1} for winter and summer specific mass balance, respectively (the uncertainty range is $\pm$ 1 standard deviation). Regions with the highest RMSE for winter mass balance are North Asia (RMSE = 1.70 m w.e. year^{-1}), Alaska (1.58 m w.e. year^{-1}), Western Canada and US (1.46 m w.e. year^{-1}), while the highest RMSE for summer mass balance are derived for Caucasus (2.08 m w.e. year^{-1}), Western Canada and US (1.86 m w.e. year^{-1}), and Alaska (1.63 m w.e. year^{-1}). These values are high but they are assessed over a small fraction of glaciers in a region. The average bias for the annual mass balance is -0.3 $\pm$ 0.5 m w.e. year^{-1}, where all but three regions (Arctic Canada North, Greenland and Central Asia) have negative bias, indicating that the modeled annual mass balance is more negative than the observed. Finally, ten out of the 14 regions show significant correlation (t test, 95 % confidence interval) between the modeled and observed annual specific mass balances. The results of the validation are further used in the assessment of uncertainties (Sect. 4.4.2) where we propagate the RMSE of each region to quantify a bulk error in the regional and global projections of volume loss.

As an additional analysis of model performance, we compare our modeled ice loss to the geodetically-derived ice loss of two regions where losses by calving can be assumed small: (1) Swiss Alps (Paul and Haeberli 2008) and (2) British Columbia (Schiefer et al. 2007). For (1), Paul and Haeberli (2008) used two different methods for calculating the mean cumulative mass balance for about 1,050 glaciers in the Swiss Alps; the total glacierized area

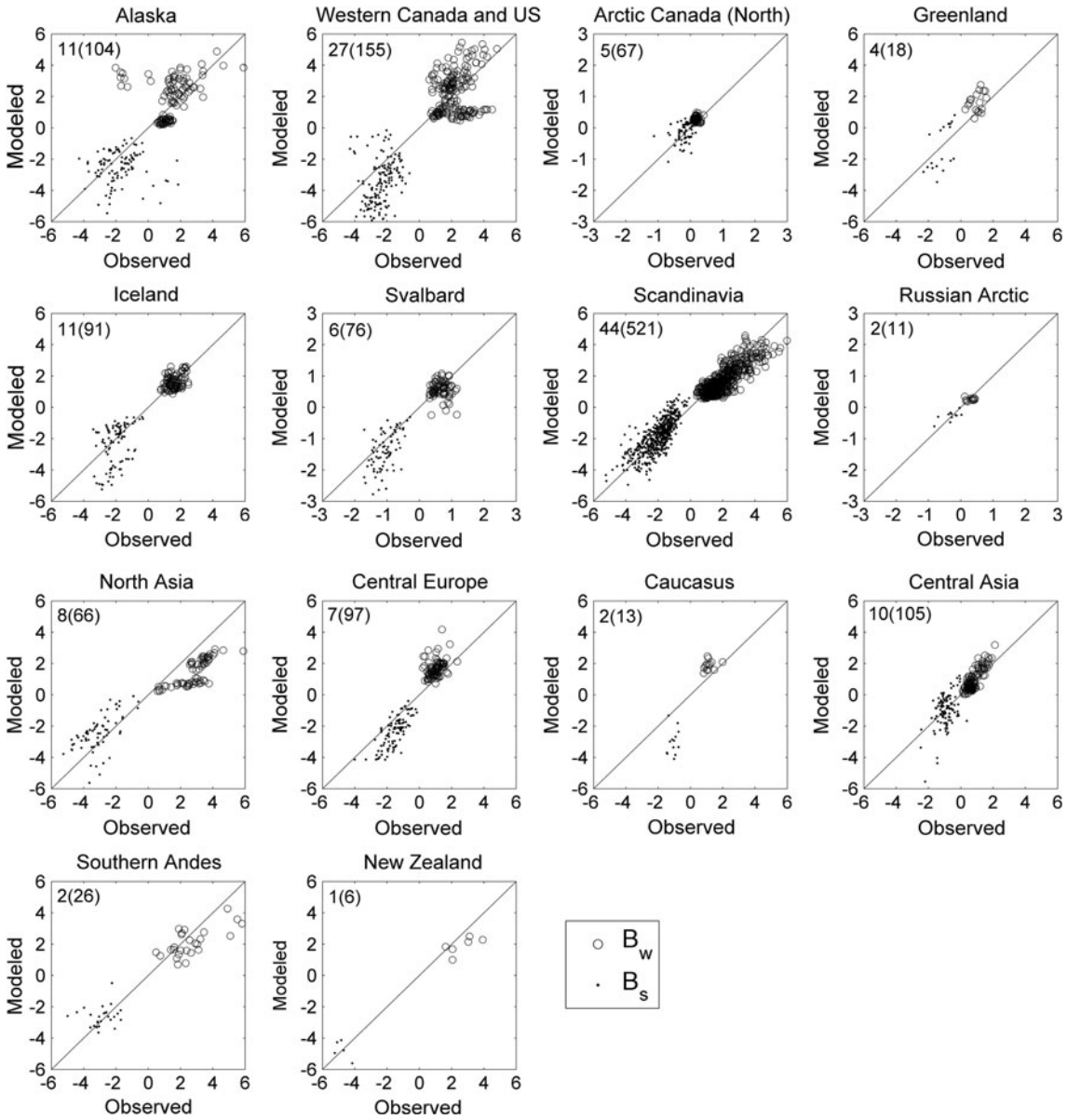

Fig. 3 Modeled versus observed specific winter (B_w) and summer (B_s) mass balances in m w.e. year $^{-1}$ for individual glaciers of the 14 regions and years for which observations are available. Observations are from the compilation of Dyurgerov (2010). In the *upper left corner* of each plot is the number of glaciers and (*in parentheses*) the total number of observations per season

is not reported. Their results yielded −7 and −11 m w.e. of glacier thinning over the period 1985–1999. We extracted and ran the mass balance model for all glaciers from the RGI that belong to the region of Swiss Alps, giving us a total of 888 glaciers (individual glacier area >0.1 km^2). For the same period of 1985–1999, we obtain cumulative mass loss of −4.8 m w.e.. For (2), over the same period, Schiefer et al. (2007) quantified the thinning of all glaciers in British Columbia to be −11.70 ± 2.85 m w.e.. Running the mass balance model over all glaciers in British Columbia, we calculate cumulative mass loss of −6.30 m w.e.. The large difference can be partially explained by the mismatch between total area of glaciers in this region: while Schiefer et al. (2007) derived their result using 28,826 km^2 of glacierized area for 1985, our total area of all Western Canadian glaciers from the RGI is half the size (14,505 km^2).

3.4 Model for ice dynamics

An ideal simulation of the dynamic response of glaciers to climate change would couple a physically-based ice flow model to a surface mass balance model. However, physically-based ice flow models require more input data than currently available on a global scale. For example, required

Table 3 Results from the model validation for annual, a, winter, w, and summer, s, specific mass balance: root-mean-square-error (RMSE), difference between the modeled and observed specific mass balance averaged over the glacier sample (Bias), and the correlation between modeled and observed specific mass balances for each region (r)

Region	RMSE a (m w.e.year^{-1})	RMSE w (m w.e.year^{-1})	RMSE s (m w.e.year^{-1})	Bias a (m w.e.year^{-1})	Bias w (m w.e.year^{-1})	Bias s (m w.e.year^{-1})	r a	r w	r s
Alaska	2.27	1.58	1.63	−0.26	**0.46**	**−0.72**	**0.40**	**0.25**	0.06
Western Canada and US	2.37	1.46	1.86	**−1.04**	0.10	**−1.13**	**0.41**	0.12	**0.25**
Arctic Canada (North)	0.35	0.14	0.32	**0.16**	**0.11**	0.05	**0.27**	0.03	**0.28**
Greenland	1.43	0.86	1.15	0.52	**0.63**	−0.11	0.06	0.33	**0.58**
Iceland	1.33	0.47	1.25	−0.32	0.01	**−0.32**	**0.33**	**0.37**	**0.39**
Svalbard	0.69	0.36	0.59	**−0.42**	**−0.09**	**−0.32**	0.20	−0.05	**0.54**
Scandinavia	1.37	0.98	0.96	−0.09	**−0.26**	**0.17**	**0.56**	**0.50**	**0.52**
Russian Arctic	0.22	0.12	0.18	−0.02	−0.05	0.03	**0.75**	0.05	**0.67**
North Asia	2.17	1.70	1.35	**−0.82**	**−1.32**	**0.50**	0.22	0.20	**0.34**
Central Europe	1.33	0.84	1.03	−0.16	**0.65**	**−0.81**	**0.76**	**0.36**	**0.75**
Caucasus	2.24	0.83	2.08	**−1.19**	**0.74**	**−1.93**	**0.66**	0.27	0.15
Central Asia	1.05	0.46	0.94	0.05	**0.14**	−0.09	**0.21**	**0.75**	**0.47**
Southern Andes	1.48	1.12	0.96	-0.27	−0.54	0.27	**0.60**	**0.69**	0.16
New Zealand	1.22	0.93	0.80	−0.56	−0.72	0.16	0.27	0.69	0.01

Value for Bias in bold font are statistically significant at 95 % confidence level (two-sample *t* test for equal means) meaning that the modeled mean is significantly different from the observed mean of a sample. Correlation values in bold font are statistically significant (*t* test; p value < 0.05)

input data includes ice thickness which is available for fewer than 1 % of glaciers in the world. Here we use a simplified approach which employs a scaling relationship between glacier volume and glacier length, to capture the feedback between glacier mass balance and changes in glacier hypsometry (e.g. glacier-wide mass loss is expected to slow down as the glacier retreats from low-lying, high-ablation altitudes; Huss et al. 2012). Radić et al. (2007, 2008) investigated the application of the scaling relations for glaciers that are not in a steady state, but responding to some hypothetical climate change. They found that, when compared to the volume evolution from a 1-D ice flow model, scaling, especially volume-length scaling, performs satisfactorily. Following the same approach as in Radić et al. (2008), we derive glacier length from volume-length scaling, defining glacier length by the glacier altitude range. As modeled glacier volume evolves, we adjust the length by removing/adding elevation bands at the terminus. In case of glacier retreat the area change is computed from the area-altitude distribution of the lost elevation bands. In case of glacier advance the length is allowed to increase while the normalized area-elevation distribution is kept unchanged.

3.5 Downscaling of GCMs

The inability of GCMs to represent subgrid-scale features leads to biases in the climate variables at the local glacier scale. Following the statistical downscaling approach of Radić and Hock (2006) we shift the future monthly temperature time series for each GCM grid cell containing glaciers by the average bias for each month between the GCM and ERA-40 temperatures over the period 1980–1999. In contrast to Radić and Hock (2011) who downscaled precipitation on an annual basis, here the bias is corrected on a monthly basis. For each month the GCM precipitation is scaled with a monthly correction factor between VASClimO precipitation climatology and GCM mean monthly precipitation over 1980–1999. Thus, for both climate variables we correct seasonality in the GCMs relative to seasonality in the reanalysis and climatology dataset.

3.6 Model spin-up and projections

Because the model calibration is performed over the period 1961–2000, while the future climate forcing is given for 2006–2100, we use the gap between the two periods to spin-up our model. We choose to start the model run at 2001, forcing it until 2005 with the downscaled historical scenarios of temperature and precipitation from the same ensemble of GCMs. The glacier geometry for the year 2001 is from the RGI since this dataset mostly consists of glacier outlines compiled within the last decade (Arendt et al. 2012). In the spin-up period we truncate the first 2 years of results because the initial snow depth (at 2001) on each glacier is set to zero, making the initial modeled mass balances unreliable. Thus, the volume evolutions are

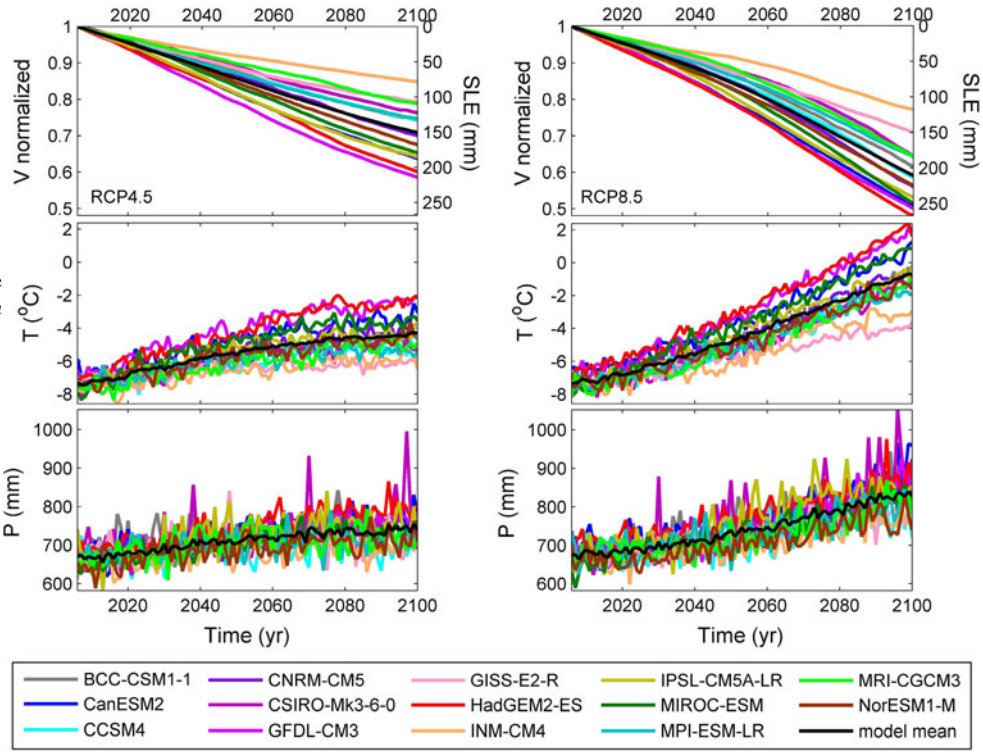

Fig. 4 Projected normalized annual volume of all glaciers, *V*, and corresponding sea-level equivalent, SLE, of the volume change for 2006–2100 in response to 14 GCM scenarios based on two emission scenarios (RCP4.5 *left side*, RCP8.5 *right side*), projections of annual mean temperature, and annual precipitation from all GCMs, where the time series are averaged over the glacierized area. *Black curve* in *each plot* is the mean of the ensemble

provided for 2003–2100, while for the presentation of results we focus on the period 2006–2100 as this is when the actual RCP forcing is applied in the GCMs.

4 Results and discussion

4.1 Global glacier volume change 2006–2100

The ensemble of projections with 14 GCMs and the RCP4.5 and RCP8.5 scenarios shows substantial glacier volume losses (Fig. 4). The multi-model mean for global volume loss over 2006–2100 is 155 ± 41 mm SLE (sea-level equivalent) for RCP4.5, and 216 ± 44 mm SLE for RCP8.5 (multi-model mean ± one standard deviation). The large standard deviations reflect our model's sensitivity to the forcing GCM. For RCP4.5 global volume losses range from 15 to 41 %, corresponding to 82–218 mm SLE, while for RCP8.5 volume losses range from 23 to 52 % corresponding to 122–272 mm SLE. All 14 GCMs project an increase in annual mean temperatures averaged over all grid cells containing glaciers: the difference between the 20-year mean temperature at the end of the century (2081–2100) and at the beginning (2003–2022) is 2.7 ± 0.8 K for RCP4.5 (multi model mean ± one standard deviation) and 5.7 ± 1.2 K for RCP8.5. For comparison, the same difference derived from 10 GCMs with A1B emission scenario, used in Radić and Hock (2011), is 3.2 ± 0.7 K. Precipitation is projected to increase in each GCM, where the 20-year mean precipitation at the end of the century is 10 ± 4 % (RCP4.5) and 21 ± 4 % (RCP8.5) larger than at the beginning. Using 10 GCMs with A1B scenario gives a multi-model increase in precipitation of 11 ± 5 %.

In comparison with Radić and Hock (2011), who projected 127 ± 37 mm SLE over 2001–2100, we arrive at higher projections of SLE over a slightly shorter period. To achieve a more consistent comparison with the former study, we force our mass balance model with the A1B scenario from the same 10 GCMs used in Radić and Hock (2011) and project 150 ± 37 mm SLE. This SLE projection in response to midrange A1B scenario agrees well with our projection for RCP4.5, which is also a midrange scenario. Although we share the same mass balance model as in Radić and Hock (2011), the mismatch between the projected SLE for the same climate forcing (A1B emission scenario) is mainly due to significant differences in glacier input data (e.g. new glacier inventory versus incomplete glacier inventory in former study; real glacier hypsometry versus assumed hypsometry in former study) and model initialization (e.g. C09 estimates of regional mass balance versus regional mass balance from Dyurgerov and Meier (2005) in the former study). Additionally, our initial global glacier volume of 520 mm SLE, assessed by volume-area scaling (Sect. 2.1), is smaller by 80 mm SLE than in the former study.

4.2 Regional volume change 2006–2100

Volume change (as a percentage of initial volume) varies considerably among the 19 regions and among the GCMs (Fig. 5). The ensemble projections for RCP4.5 range between a mass gain of 7 % (Iceland) and a 99 % volume loss (Scandinavia), while for RCP8.5 they range between 9 % volume loss (Arctic Canada North) and 100 % volume loss (Scandinavia, Central Europe, Low Latitudes). The largest range of volume projections by 2100 among the 14 GCMs is found in Iceland (+7 to −97 % volume change for RCP4.5, and 9–98 % volume loss for RCP8.5), Scandinavia (13–99 % volume loss for RCP4.5, and 66–100 % for RCP8.5), and South Asia West (4–75 % volume loss for RCP4.5, and 34–87 % for RCP8.5). The smallest range of volume projections, indicating good agreement in projected climate among the 14 GCMs, is found in Antarctic and Subantarctic (12–28 % volume loss for RCP4.5, and 14–38 % for RCP8.5), Low Latitudes (78–97 % volume loss for RCP4.5, and 93–100 % for RCP8.5), and Caucasus (72–97 % volume loss for RCP4.5 and 90–99 % for RCP8.5).

The regions that are projected to lose more than 75 % of their current volume on average are, for RCP4.5: Western Canada and US (85 ± 11 %), Scandinavia (76 ± 25 %), North Asia (88 ± 7 %), Central Europe (84 ± 10 %), Caucasus (89 ± 7 %) and Low Latitudes (88 ± 6 %). For RCP8.5 all of these regions lose on average more than 90 % of their current volume by 2100. In comparison to other regions, the regions with large percentage volume loss have numerous small glaciers whose wastage has a negligible effect on global sea-level rise. Nevertheless, their glaciers have a significant role in regional water resources (e.g. Huss 2011; Kaser et al. 2010), which will change substantially if most glaciers disappear by 2100 as projected.

The main contributors to global volume loss by 2100 are Arctic Canada (41 ± 15 mm SLE for RCP4.5, 57 ± 18 mm SLE for RCP8.5), Antarctic and Subantarctic (22 ± 6 mm SLE for RCP4.5, 29 ± 8 mm SLE for RCP8.5), Russian Arctic (20 ± 8 mm SLE for RCP4.5, 28 ± 8 mm SLE for RCP8.5), Alaska (18 ± 7 mm SLE for RCP4.5, 25 ± 8 mm SLE for RCP8.5), High Mountain Asia (combined Central Asia, South Asia West and East; 16 ± 5 mm SLE for RCP4.5, 22 ± 4 mm SLE for RCP8.5) and Greenland peripheral glaciers (13 ± 7 mm SLE for RCP4.5, 20 ± 7 mm SLE for RCP8.5). Most of these regions were identified in Radić and Hock (2011) as major contributors to global sea-level rise by 2100; however, our new estimates give higher SLE for all of them except Alaska. Particularly, the new SLE projections for Greenland are three to five times larger than in the previous study, which derived 4 ± 2 mm SLE, while for High Mountain Asia the new results are five to seven times larger than before (3 ± 5 mm SLE in Radić and Hock (2011)). In case of Greenland, the large difference in the projections between the two studies is most probably due to different inventories and total glacierized area: while Radić and Hock (2011) upscaled their modeled mass changes to an estimated total area of 54,400 km^2 (Radić and Hock, 2010), this study modelled glaciers over a much larger area (87,810 km^2; Table 1). For High Mountain Asia, in addition to differences in the inventories, the choice of precipitation downscaling may also significantly affect the projections: while Radić and Hock (2011) corrected only for the annual bias in GCMs, here we corrected for the seasonal cycle (Sect. 3.5).

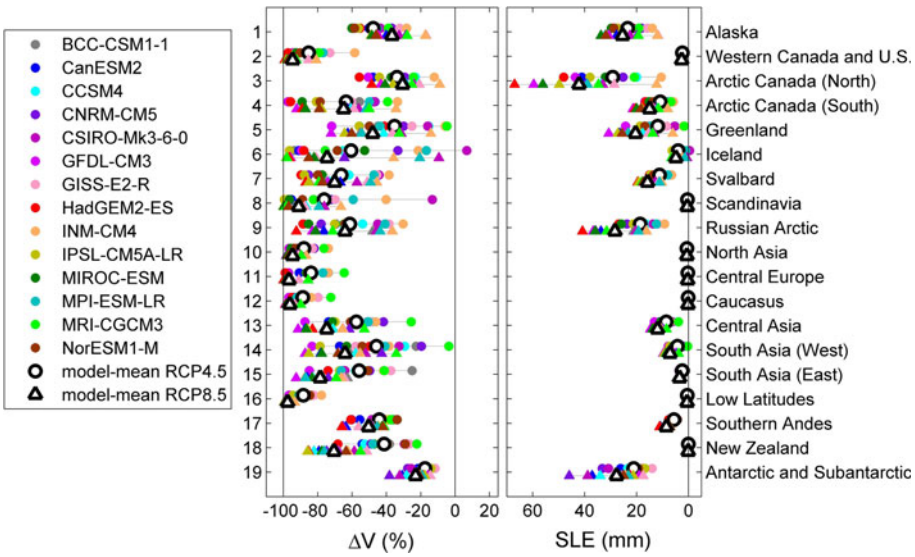

Fig. 5 Total volume change over 2006–2100, ΔV, expressed in percentage of initial volume of all glaciers within each region, and in sea-level equivalent, SLE. Results are presented for *19 regions* based on temperature and precipitation projections from 14 GCMs forced by RCP4.5 (*circles*) and RCP8.5 (*triangles*)

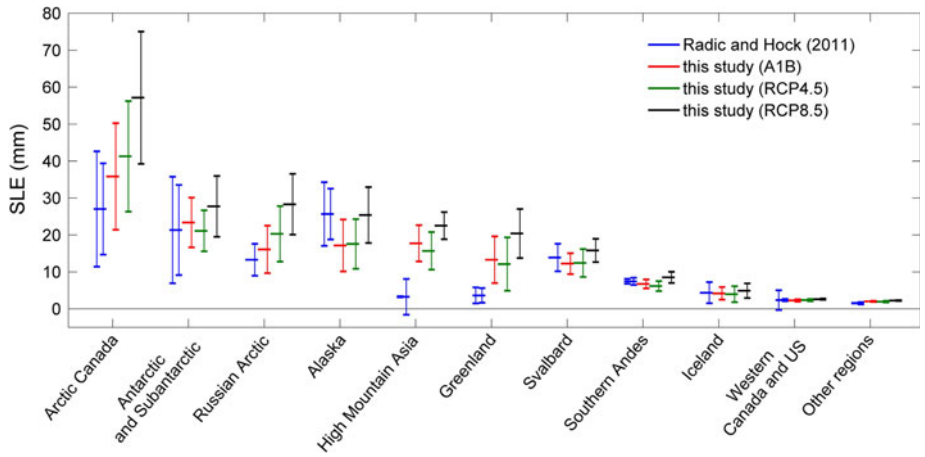

Fig. 6 Regional volume change (SLE) over the twenty-first century: mean over GCMs (*longest horizontal lines*) and uncertainty range (*upper and lower horizontal lines*). In *blue* are estimates from Radić and Hock (2011) showing uncertainty due to incomplete glacier inventory at the time of assessment (*left blue bar*) and a standard deviation from ten GCMs with A1B emission scenario (*right blue bar*). The *other colors* show results from this study, where the uncertainty *bar* represents a standard deviation from the same ten GCMs (A1B) as in Radić and Hock (2011; *red bar*), and 14 GCMs with RCP4.5 (*green bar*) and RCP8.5 (*black bar*). For the purpose of comparison with Radić and Hock (2011) some of the *19 regions* are combined into one: Arctic Canada North and South into "Arctic Canada", and Central Asia, South Asia West and East into "High Mountain Asia"

In Fig. 6 we compare our regional SLE projections (including the runs with A1B emission scenarios from 10 GCMs) with those in the former study, showing the model mean and uncertainty for each region with significant contribution to global volume loss. For the former estimates we also illustrate the uncertainty due to the statistical upscaling applied in each region that had an incomplete glacier inventory at the time. This was the dominant uncertainty source, not only for the model-mean, as plotted in the figure, but for each projection from GCMs. The new estimates are free of this uncertainty, since the inventory is now complete; however, the large uncertainty bars due to the choice of GCM remain similar to those in the former study or become even larger for some regions (e.g. for Arctic Canada, Russian Arctic and Greenland).

In Fig. 7 we plot the volume evolution for 2006–2100 for each GCM (RCP4.5) and for each of the 19 regions. The characteristic features are the large scatter of volume projections among the 14 GCMs, and different rates of volume decrease. The large scatter in the projections among the 14 GCMs depends on the ensemble range in temperature and/or precipitation projections for a given region, but also on the sensitivity of glacier mass balance to temperature and precipitation changes in the region. To address the former, in Fig. 8 we illustrate temperature and precipitation change as a difference between the 20-year mean (2003–2022 and 2081–2100) for each GCM and each region. The largest ranges in projected temperature increase among the GCMs are for Russian Arctic, Arctic Canada and Svalbard. These regions, together with Central Asia and South Asia West, also have the largest ranges in projected precipitation increase although the large range for Central Asia (RCP4.5 and RCP8.5) is due to one outlier.

4.3 Regional volume and mass-balance sensitivities

To illustrate regional differences in sensitivity of volume change to temperature change, we plot the time-series of normalized annual volume against the time series of temperature anomalies (annual deviations from the 1981–2000 mean temperature) for each region (Fig. 9), or in other words, regional $V(t)$ against regional $\Delta T(t)$. Both time series represent multi-model means from the 14 GCMs. The slope of the curve tells us how fast a region is losing the total volume of its glaciers as a function of amount of warming. For the initial 2 K of warming, regions that lose glacier volume relatively rapidly are Western Canada and US, Scandinavia, North Asia, Central Europe, Caucasus and Low Latitudes. On the other hand, regions with relatively low regional volume sensitivity to the initial 2 K of warming are Arctic Canada (North), Russian Arctic, Antarctic and Subantarctic, Greenland, Alaska and Svalbard. What causes these differences in regional volume response to warming? The answer lies partially in the sensitivity of glacier mass balance to temperature (and precipitation) changes, but also in the size distribution and hypsometry of the glaciers. For example, if a regional glacier volume consists mostly of low-altitude small glaciers whose mass balance is highly sensitive to temperature changes, the response of the regional volume to warming is expected to be faster than in a region where this is not the case. To

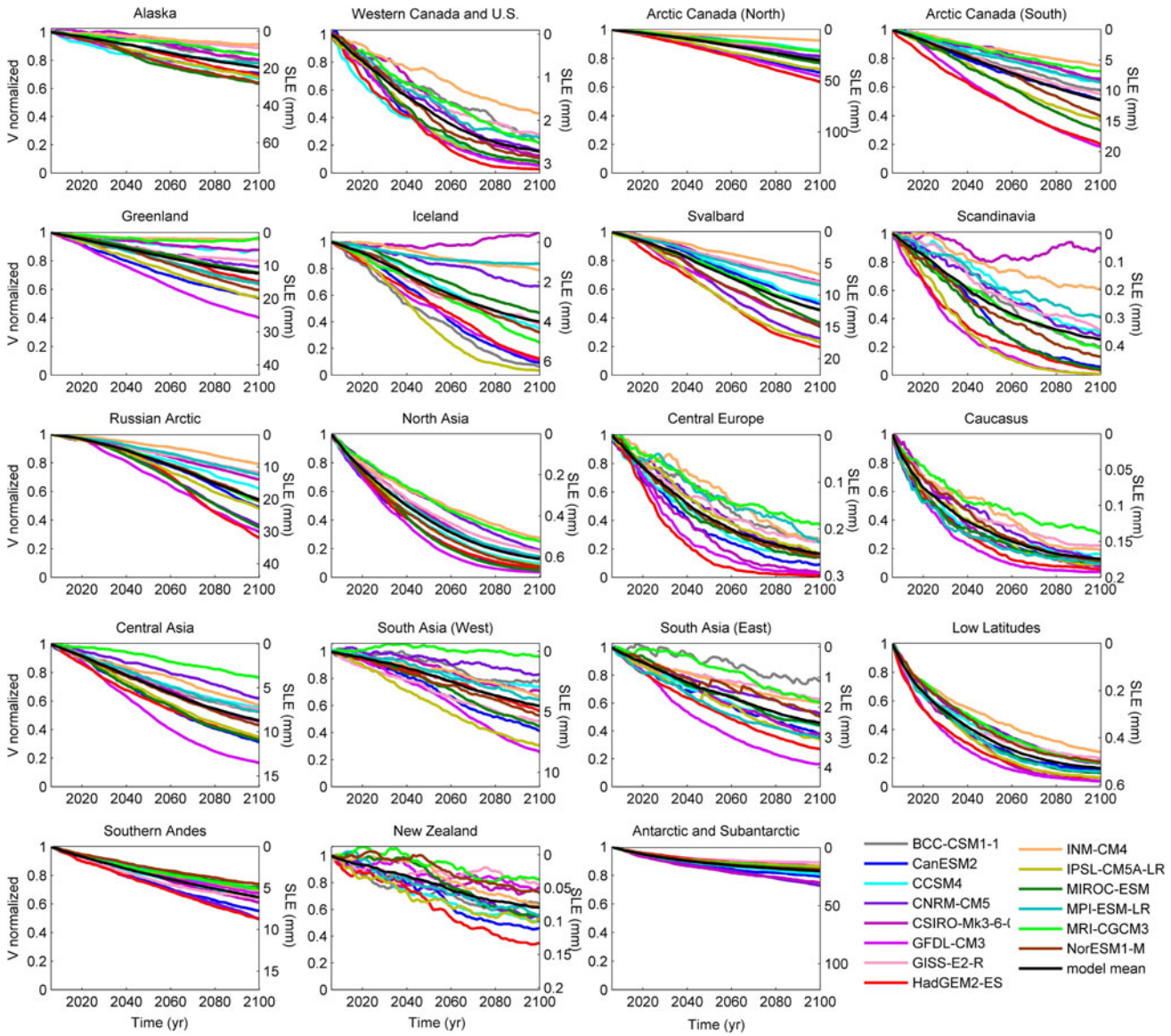

Fig. 7 Projected normalized annual volume, *V*, and corresponding sea-level equivalent, SLE (mm), for each of the *19 regions*, in response to 14 GCM scenarios forced by RCP4.5 for the period 2006–2100

illustrate the regional variability of glacier sizes and hypsometries, we plot the distribution of glacierized area (in percent of regional glacierized area) with elevation, separately for each glacier elevation band, where the elevation interval is 20 m (Fig. 10). Combining the information from Fig. 9 and 10, we find that a region with relatively high regional volume sensitivity is one whose small glaciers (individual glacier area <1 km^2) account for a relatively large percentage (>20 %) of the regional glacierized area. Also, the distribution of glacierized area for such a region is skewed toward small glaciers (i.e. with elevation range < 200 m), many of which are located at relatively low altitudes (Fig. 10). On the other hand, a region with relatively low regional volume sensitivity has, at present, very few small glaciers, for example: Alaska (total area of its small glaciers is 6 % of regional glacierized area), Arctic Canada North (1 %), Greenland (5 %), Svalbard (1 %), Russian Arctic (0.2 %) and Antarctic and Subantarctic (0.3 %). Furthermore, as illustrated in Fig. 9, the rate of regional volume response to warming, for a given region, is not a constant. It is expected that, as the distribution of glacier area and hypsometry changes, so too does the response rate to warming.

Next we analyse the sensitivity of regional glacier mass balance, using specific units (m w.e. $year^{-1}$) indicating the regional water-equivalent thinning/thickening rates in response to regional temperature and precipitation changes. Regional averages are area-weighted averages of all glaciers

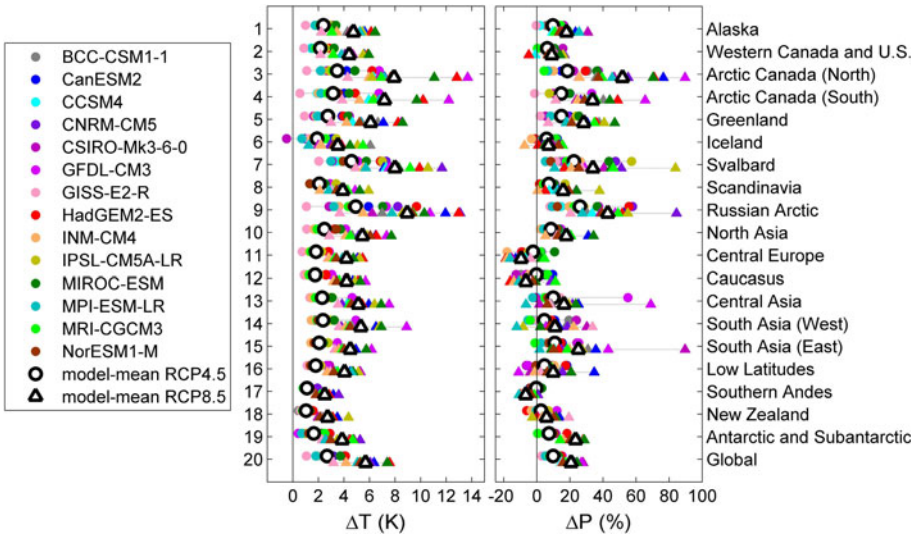

Fig. 8 Difference between the 20-year mean temperature at the end of the century (2081–2100) and the beginning of the century (2003–2100), ΔT, and difference between the 20-year mean precipitation for the same periods, ΔP (expressed as % change relative to the mean precipitation over 2003–2100) from 14 GCMs forced by RCP4.5 (*circles*) and RCP8.5 (*triangles*)

within a region. With the assumption that the regional mass balance is a function of annual temperature and precipitation, we can write the following equation:

$$\Delta B = \frac{\partial B}{\partial T}\Delta T + \frac{\partial B}{\partial P}\Delta P \quad (4)$$

where ΔB is the change in regional mass balance, here derived as the difference between the modeled mean regional mass balance over 2081–2100 and the mean over 2003–2022, ΔT and ΔP are temperature and precipitation change, respectively, between the two periods, while $\partial B/\partial T$ and $\partial B/\partial P$ are the regional mass balance sensitivities to temperature and precipitation change, respectively. $\partial B/\partial T$ is derived from linear regression between annual specific mass balance, $B(t)$ and annual mean temperature, $T(t)$, in a model run in which the precipitation forcing is approximately kept constant in time (i.e. iterated 20 years of $P(t)$ from 1981 to 2000 throughout the twenty-first century). Similarly, $\partial B/\partial P$ is derived from linear regression between annual specific mass balance, $B(t)$, and annual mean precipitation, $P(t)$, in a model run in which the temperature forcing is kept constant in time (i.e. iterated 20 years of $T(t)$ from 1981 to 2000 throughout the twenty-first century). Therefore, the estimated mass balance sensitivity to long-term temperature change is approximately independent of long-term precipitation change and vice versa.

Table 4 shows the values for each variable in Eq. (4), all derived as means of an ensemble of three GCMs (GFDL, INM and MPI-ESM-LR) that cover the simulated global range of projections (GFDL projected the largest volume loss, INM the smallest, while the MPI-ESM-LR is the closest to the ensemble mean of the 14 GCMs). Global glacier mass change between the periods 2081–2100 and 2003–2022 is -75 ± 39 m w.e. (model mean $\pm$ one standard deviation). The region with the greatest mass loss, according to these three GCMs, is North Asia (-153 ± 68 m w.e.), while the smallest mass loss is projected for New Zealand (-21 ± 9 m w.e). For most of the regions, the change in regional mass balance, ΔB, is negative, which means that the regional mass balance by the end of the century becomes more negative than it was at the beginning of the century. There are four regions where ΔB is positive: North Asia (0.8 ± 0.2 m w.e. year^{-1}), Caucasus (0.9 ± 0.4 m w.e. year^{-1}), Low Latitudes (0.5 ± 0.3 m w.e. year^{-1}) and Antarctic and Subantarctic (0.4 ± 0.5 m w.e. year^{-1}), while on the global scale ΔB is -0.2 ± 0.3 m w.e. year^{-1}. The most probable explanation for the positive ΔB, while the glaciers in a region are losing mass, is that the majority of glaciers have already passed their peak negative mass balances. Also, this might mean that the glaciers are reaching a new equilibrium in the changing climate. On the other hand, a region with negative ΔB may indicate that (1) the region has a large low-elevation glacierized area which is shrinking more slowly than it is thinning and/or (2) the retreating glaciers cannot reach a new equilibrium because the equilibrium line altitude is above their maximum elevations.

The majority of regions have statistically significant negative $\partial B/\partial T$, especially New Zealand (-0.56 m w.e. year^{-1} K^{-1}), and Central Europe (-0.51 mm w.e. year^{-1} K^{-1}), while the global mean is -0.16 ± 0.08 m w.e. year^{-1} K^{-1}. Our values for $\partial B/\partial P$ confirm previous findings (e.g. de Woul and Hock, 2005) that a specific mass balance sensitivity to warming of +1 K is larger than to +10 % increase in precipitation. The regions with the most positive, statistically significant $\partial B/\partial P$ are Western Canada and US [0.32 m w.e. year^{-1} (10 %)$^{-1}$] and Scandinavia [0.26 m w.e. year^{-1} (10 %)$^{-1}$], while the global mean is 0.10 ± 0.02 m w.e. year^{-1} (10 %)$^{-1}$. While most regions experience temperature increases larger than 2 K per century, precipitation is rarely projected to increase more than

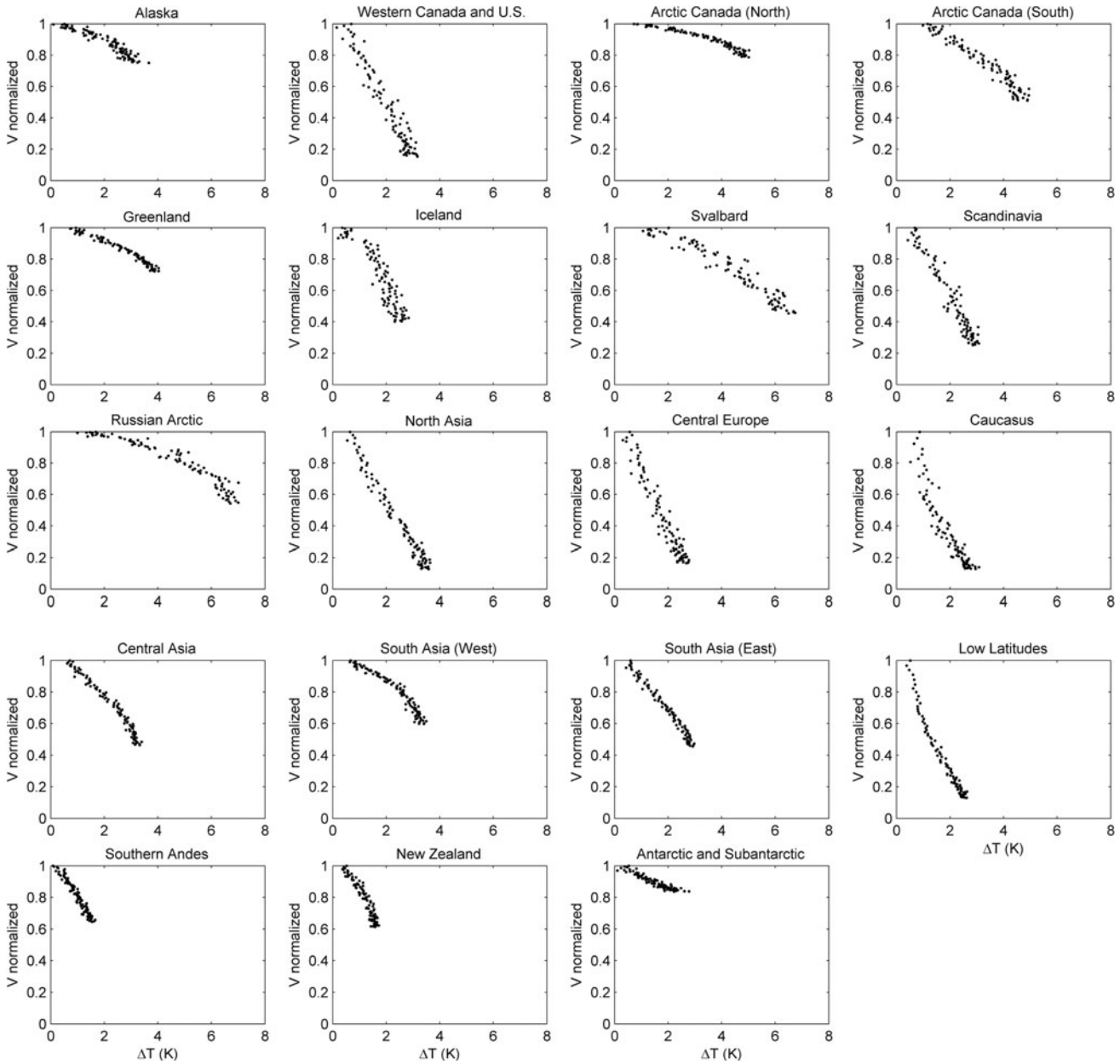

Fig. 9 Projected time series of annual normalized regional volume, $V(t)$, versus time series of annual regional temperature anomalies, $\Delta T(t)$ averaged over glacierized area, with respect to the 1981–2000 temperature mean. Both time series are represented by the ensemble mean of 14 GCMs (RCP4.5) where t goes from 2006 to 2100 (i.e. 95 dots for each region). $V(t)$ are normalized relative to the initial regional volume at $t = 2006$, so that $V(2006) = 1$ while $\Delta T(2006)$ is close to zero

15 % per century. We note that these sensitivities are derived with the assumption that the changes in annual mass balance are only dependent on the changes in annual temperature and precipitation, ignoring seasonal effects.

For the last step of analysis, we decompose the annual temperature and precipitation changes (ΔT and ΔP in Eq. 4) into summer and winter changes in order to identify which season dominates the change in the annual mean. Summer, or ablation season, is represented by the months April to September for the Northern Hemisphere and October to March for the Southern Hemisphere, while the other 6 months represent winter or accumulation season. In addition, we also look into the changes of continentality index, which is the range of the annual temperature cycle. Larger continentality index means larger amplitude of the temperature seasonal cycle, and therefore more continental climate. For example the continentality index at the present day is $\sim$35 K for Arctic Canada North and $\sim$9 K for New Zealand. The results for temperature change show that,

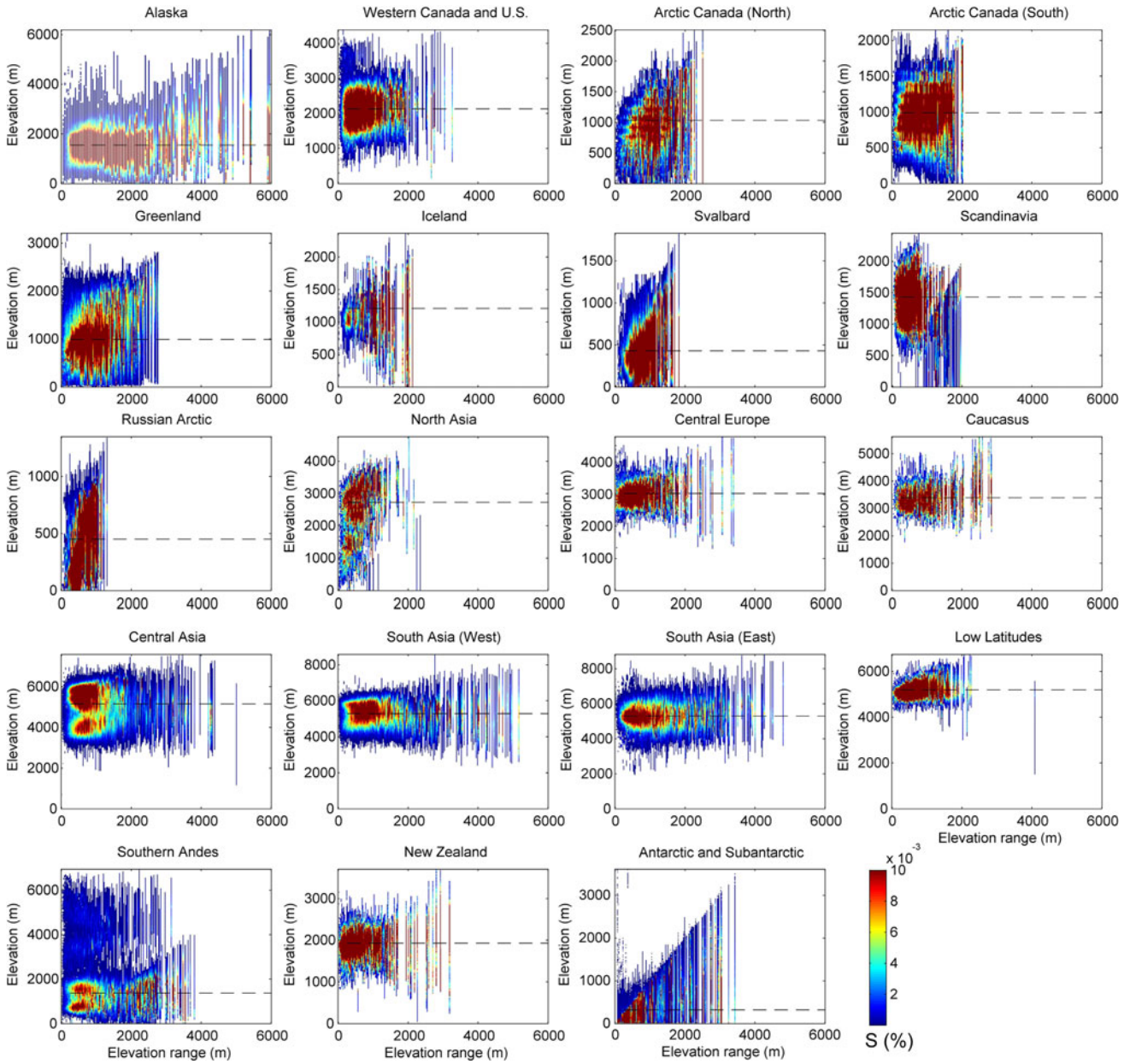

Fig. 10 Glacierized area (*colors*; in % of regional glacierized area) plotted against elevation (y-axis) and glacier elevation range (x-axis). Bins for elevation range (x-axis) and elevation (y-axis) increase with a step of 20 m (25 m for Alaska). Area (%) is represented by a *color bar*: e.g. *red color* indicates where the most of glacierized area is located. In general, glaciers with smaller elevation range are also smaller in size. Glacierized area that extends down to sea level (elevation = 0 m) often indicates presence of tidewater glaciers (e.g. Greenland, Antarctic and Subantarctic). The *horizontal dashed line* shows the median elevation of the regional glacier hypsometry

especially for Arctic Canada North and South, Svalbard, and Russian Arctic, winter months warm by more than summer months, which reduces the continentality index. In other words, the climate regime as represented by temperature seasonality is projected to become more maritime in the Arctic regions. On a global scale, over glacierized regions, the continentality index dropped by -1.7 ± 0.6 K. Regions where the summer warming is significantly larger than the winter warming are Central Europe and Caucasus, both of which are projected to lose more than 80 % of their current glacier volume by 2100 (as a mean of three GCMs in this analysis). Regions with the largest projected warming (e.g. the Arctic regions) are also projected to have the largest increase in precipitation. For the Arctic regions (Arctic Canada North and South, Svalbard, Russian Arctic) more than half of the increase in annual precipitation occurs during the winter months (October to March). We extend the analysis of seasonality changes to all 14 GCMs (Fig. 11)

Table 4 Regional glacier mass change between the periods 2003–2022 and 2081–2100, $\int$ Bdt (m w.e.), change in regional mass balance between the two periods, ΔB (m w.e. year^{-1}), sensitivity of regional mass balance to temperature change derived from the period 2003–2100, $\partial B/\partial T$ (m w.e. year^{-1} K^{-1}), change in annual temperature, ΔT (K), and in temperature averaged over April to September, $\Delta T_{A\text{-}S}$(K), between the two periods, sensitivity of regional mass balance to precipitation change, $\partial B/\partial P$ [m w.e. year^{-1} (10 %)$^{-1}$], change in annual sums of precipitation, ΔP (%) and in precipitation summed over October to March, ΔP_{O-M} (%) between the two periods, and change in continentality index, CI (K), between the two periods

Region	$\int$ Bdt (m w.e.)	ΔB (m w.e. year^{-1})	∂B/∂T (m w.e. year^{-1} K^{-1})	ΔT (K)	$\Delta T_{A\text{-}S}$ (K)	∂B/∂P (m w.e. year^{-1}10 %)$^{-1}$	ΔP (%)	ΔP_{O-M} (%)	ΔCI (K)
Alaska	−65 ± 37	−0.3 ± 0.3	**−0.29** ± 0.06	2.2 ± 0.5	0.9 ± 0.3	**0.17** ± 0.05	10 ± 3	6 ± 2	−1.2 ± 0.9
W Canada and US	−91 ± 43	−0.1 ± 0.3	**−0.30** ± 0.05	2.0 ± 0.6	1.0 ± 0.4	**0.32** ± 0.03	7 ± 1	6 ± 1	−0.4 ± 1.5
Arctic Canada (N)	−90 ± 49	−0.3 ± 0.4	−0.15 ± 0.10	3.7 ± 2.1	1.1 ± 0.7	0.03 ± 0.01	15 ± 10	8 ± 4	−3.8 ± 2.1
Arctic Canada (S)	−132 ± 100	0.0 ± 0.1	**−0.24** ± 0.13	3.6 ± 2.2	1.2 ± 0.8	**0.10** ± 0.03	18 ± 7	7 ± 5	−3.3 ± 1.4
Greenland	−59 ± 46	−0.3 ± 0.3	−0.09 ± 0.08	2.7 ± 1.2	0.9 ± 0.5	**0.18** ± 0.04	12 ± 3	5 ± 2	−1.7 ± 1.3
Iceland	−102 ± 91	−0.1 ± 0.2	−0.34 ± 0.37	1.5 ± 0.7	0.6 ± 0.4	0.11 ± 0.05	2 ± 4	1 ± 2	-0.7 ± 0.8
Svalbard	−115 ± 55	−0.1 ± 0.2	**−0.22** ± 0.10	4.2 ± 0.9	1.3 ± 0.4	**0.08** ± 0.02	15 ± 7	9 ± 7	−3.9 ± 3.5
Scandinavia	−72 ± 53	−0.3 ± 0.1	**−0.36** ± 0.11	2.0 ± 0.7	0.9 ± 0.4	**0.26** ± 0.10	7 ± 1	3 ± 2	−0.7 ± 0.7
Russian Arctic	−122 ± 79	−0.4 ± 0.4	**−0.27** ± 0.11	4.7 ± .8	1.3 ± 0.7	**0.06** ± 0.01	19 ± 8	13 ± 5	−4.8 ± 1.4
North Asia	−153 ± 68	0.8 ± 0.2	−0.14 ± 0.10	2.6 ± 1.1	1.2 ± 0.5	0.16 ± 0.11	7 ± 5	4 ± 3	−0.8 ± 0.5
Central Europe	−81 ± 40	−0.1 ± 0.2	**−0.51** ± 0.22	1.9 ± 0.7	1.1 ± 0.4	0.13 ± 0.02	−8 ± 8	1 ± 1	1.9 ± 0.9
Caucasus	−94 ± 31	0.9 ± 0.4	−0.28 ± 0.25	1.8 ± 0.9	1.0 ± 0.5	0.09 ± 0.07	−3 ± 3	3 ± 2	1.2 ± 1.1
Central Asia	−71 ± 44	−0.4 ± 0.4	**−0.21** ± 0.06	2.7 ± 1.4	1.3 ± 0.7	**0.10** ± 0.01	17 ± 20	1 ± 1	0.1 ± 0.8
South Asia (W)	−66 ± 43	−0.6 ± 0.4	**−0.31** ± 0.09	2.9 ± 1.5	1.5 ± 0.8	**0.10** ± 0.03	−2 ± 4	−3 ± 1	0.3 ± 0.8
South Asia (E)	−64 ± 31	−0.2 ± 0.4	−0.07 ± 0.04	2.3 ± 0.9	1.1 ± 0.5	**0.18** ± 0.01	11 ± 9	0 ± 1	−0.9 ± 0.6
Low latitudes	−86 ± 26	0.5 ± 0.3	0.00 ± 0.08	1.9 ± 0.5	1.0 ± 0.3	0.00 ± 0.20	2 ± 6	2 ± 3	−0.1 ± 0.5
Southern Andes	−58 ± 4	−0.1 ± 0.5	−0.12 ± 0.12	0.9 ± 0.1	0.5 ± 0.1	0.00 ± 0.06	0 ± 2	0 ± 1	0.1 ± 0.1
New Zealand	−21 ± 9	−0.7 ± 0.4	**−0.56** ± 0.20	1.0 ± 0.1	0.5 ± 0	0.06 ± 0.05	2 ± 6	2 ± 2	−0.1 ± 0.3
Antarctic and Subant.	−41 ± 5	0.4 ± 0.5	0.05 ± 0.10	0.7 ± 0.2	0.4 ± 0.1	0.07 ± 0.04	5 ± 1	1 ± 2	−0.3 ± 0.4
Global	−75 ± 39	−0.2 ± 0.3	−0.16 ± 0.08	2.6 ± 1.0	1.0 ± 0.4	0.10 ± 0.02	11 ± 5	4 ± 1	−1.7 ± 0.6

All values are derived as the mean of three GCMs (GFDL, INM and MPI-ESM-LR; Table 2) with RCP4.5. The uncertainty range is one standard deviation among the models. Values in bold font are statistically significant slopes of the linear regression (t test; p value < 0.05)

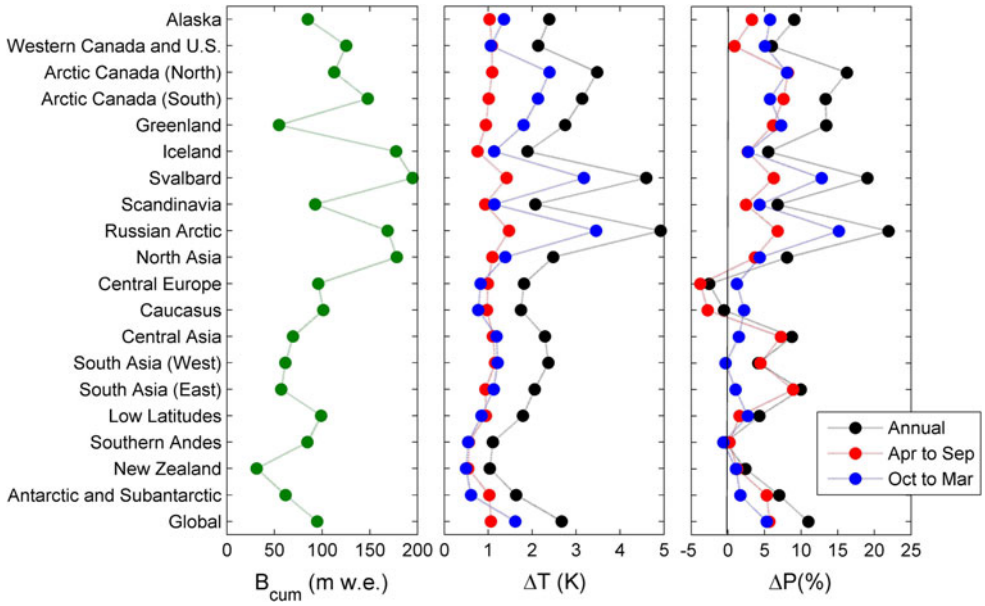

Fig. 11 Cumulative regional and global glacier mass loss over the period 2006–2100, B_{cum}, difference between the 20-year mean annual temperature for 2081–2100 and 2003–2022, ΔT, and the same for precipitation sums, ΔP (expressed as % change relative to the mean precipitation over 2003–2100). All the values are spatially averaged over the glacierized area within each region. The *black lines* are the change of the annual means, the *red lines* represent the annual mean calculated over the months April to September (i.e. sum of April to September temperatures divided by 12), and *blue lines* represent the annual mean over the months October to March (i.e. sum of October to March temperatures divided by 12). In this way, the annual value of ΔT and ΔP is the sum of the seasonal values. All the results are for the multi-model mean of 14 GCMs (RCP4.5)

which confirms the conclusions found from these three GCMs. In addition, we note that summer precipitation in both Central Europe and Caucasus is projected to decrease while winter precipitation is projected to increase. In contrast, for all the other regions, winter and summer precipitation are both projected to increase or slightly decrease. The increase in annual precipitation in High Mountain Asia (Central Asia, South Asia East and West) is strongly dominated by the increase of precipitation in summer months, or in other words during the monsoon season.

4.4 Analysis of uncertainties

4.4.1 Sensitivity tests

Following the error analysis in Radić and Hock (2011) we quantify the dominant uncertainties in the projected glacier volume loss, measured in sea-level equivalent units, with a series of sensitivity tests. Because our new estimates are free of the uncertainty due to upscaling of an incomplete glacier inventory (Fig. 7) we are mainly concerned about the uncertainties due to model performance. As shown in the previous study, the major uncertainties are due to (1) model calibration and initialization, and (2) uniform application of volume-area and volume-length scaling coefficients to all the glaciers in the world.

To quantify the uncertainty due to model calibration and initialization we rerun our mass balance model for all the glaciers using the perturbed values of one model parameter, lr_{ERA}. We chose lr_{ERA} because Radić and Hock (2011) showed that the projected SLE has the highest sensitivity to the perturbations of this parameter among all the seven parameters used for the model calibration. Also, since lr_{ERA} was used for the model initialization (i.e. minimizing the RMSE between the C09 estimated and modeled pentadal regional mass balances), running the model with different lr_{ERA} values can be seen as projecting the mass changes starting with different initial states of glacier mass balance. A perturbation of 0.1 K $(100\ \mathrm{m})^{-1}$ from the original (tuned) value of lr_{ERA}, applied to each subregion separately, is chosen in order to estimate upper and lower bounds for projected SLE (i.e. the maximum uncertainty range). This is a very large perturbation relative to plausible expectations about the sensitivity of regional mass balance to the lapse rate. For example, regional mass balance can change by 0.15 m w.e. year^{-1} ($\sim$50 % of global annual mass balance averaged over 1961–2100) with a perturbation of only 0.01 K $(100\ \mathrm{m})^{-1}$ (Radić and Hock 2011). We expect the sensitivity to this perturbation will be greater if a glacier region has greater mass balance sensitivity to temperature change ($\partial B/\partial T$). Also, the effect of the perturbation will be large in regions where the vertical distance between the elevation of the ERA-40 grid cell and the maximum glacier altitude is large: the same change in lapse rate will result in a larger total change in the temperature if the height difference is larger. Rerunning the

Table 5 Regional projections of glacier volume loss in sea-level equivalent, SLE (mm) derived for two emission scenarios RCP4.5 and RCP8.5, as a multi-model mean (first two columns after the list of regions)

Region	SLE RCP4.5	SLE RCP8.5	SLE_{high} RCP4.5	SLE_{low} RCP4.5	ΔSLE_1 RCP4.5	ΔSLE_2 RCP8.5-RCP4.5	σ RCP4.5	δ_{SLE} RCP4.5
Alaska	17.57	25.40	39.93	−2.68	22.36	7.83	6.72	4.59
Western Canada and US	2.36	2.62	2.35	1.20	1.16	0.26	0.30	0.33
Arctic Canada (North)	29.85	42.16	41.00	13.27	16.58	12.31	11.16	1.85
Arctic Canada (South)	11.44	14.99	11.81	3.46	7.98	3.55	4.25	0.90
Greenland	12.12	20.40	16.46	2.79	9.33	8.27	7.21	1.73
Iceland	3.98	4.90	4.76	−0.82	4.80	0.92	2.15	0.89
Svalbard	12.41	15.81	17.99	14.05	5.58	3.40	3.77	0.53
Scandinavia	0.37	0.45	0.45	0.08	0.29	0.08	0.12	0.05
Russian Arctic	20.29	28.31	31.49	23.73	11.20	8.02	7.53	0.40
North Asia	0.58	0.63	0.55	0.31	0.27	0.04	0.05	0.13
Central Europe	0.29	0.33	0.26	0.01	0.28	0.04	0.04	0.04
Caucasus	0.15	0.16	0.11	0.06	0.09	0.01	0.01	0.03
Central Asia	8.70	11.94	10.80	−1.57	10.27	3.24	2.46	0.38
South Asia (West)	4.52	7.09	5.68	−3.68	8.21	2.57	2.26	0.47
South Asia (East)	2.47	3.48	3.37	−2.40	4.87	1.01	0.69	0.15
Low Latitudes	0.49	0.54	0.35	−0.15	0.64	0.05	0.03	0.03
Southern Andes	6.16	8.51	12.44	0.75	6.28	2.36	1.36	1.08
New Zealand	0.08	0.14	0.13	−0.18	0.26	0.06	0.03	0.04
Antarctic and Subantarctic	21.11	27.75	39.52	24.44	18.40	6.63	5.53	5.26
Global	155	216	239	73	84	61	41	19

The next two columns contain the multi-model mean SLE projections derived from the sensitivity tests (Sect. 4.4.1) where the model parameter, lr_{ERA} is perturbed to provide upper bound estimate (SLE_{high}) and lower bound estimate (SLE_{low}). ΔSLE_1 is the larger value of the two absolute differences: SLE_{high}—SLE and SLE_{low}—SLE, approximating the error range from the sensitivity tests. ΔSLE_2 is the difference between the projected SLE from RCP8.5 and from RCP4.5, approximating the uncertainty due to the choice of RCP. σ is one standard deviation derived from the ensemble projections with 14 GCMs, approximating the uncertainty due to the choice of GCM. δ_{SLE} is the net error estimate from the error propagation (Sect. 4.4.2, Eq. 6)

model with lr_{ERA} being 0.1 K (100 m)$^{-1}$ more negative than the original, the projected ensemble mean for 2006–2100 century volume loss is 73 mm SLE (RCP4.5). For less negative lr_{ERA}, the projected volume loss is 239 mm SLE. Both values significantly differ from the original value of 155 mm SLE, representing a range of uncertainly (±84 mm SLE) which is roughly twice the standard deviation of the ensemble projections (±41 mm SLE). The sensitivity results for each of the 19 regions are listed in Table 5.

To address the uncertainties in projected volume change due to volume-length scaling, we follow the analysis in Radić and Hock (2010) where the two scaling coefficients are perturbed by prescribed error ranges. We rerun the volume projections using upper and lower bounds for the scaling constant and exponent. The change in projected global volume loss by 2100 is within ±40 mm SLE for each GCM, equivalent to the uncertainty range reported in Radić and Hock (2011). Additionally, we also quantify a potential systematic error arising from the fact that we do not differentiate between mountain glaciers and ice caps in any region except Iceland and Antarctica. To quantify what effect the volume-area scaling coefficients for ice caps would have on the total volume and projected volume change we assume that the largest ice bodies (with area larger than S_0 in Table 1) in the Arctic (Arctic Canada North and South, Alaska, Russian Arctic, Greenland, Svalbard, Scandinavia), High Mountain Asia and the Southern Andes are ice caps. With such hypothetical differentiation between mountain glaciers and ice caps we calculate the global glacier volume to be 406 mm SLE, which is lower than our original estimate by 117 mm SLE (Table 1). Rerunning the model with this modified glacier classification the projected multi-model mean for 2006–2100 century volume loss is 149 ± 37 mm SLE for RCP4.5, and 203 ± 37 mm SLE for RCP8.5. These model-mean volume losses are 6 and 13 mm SLE lower than the original ones for RCP4.5 and RCP8.5, respectively. Both differences are well within the uncertainty range due to the choice of GCM (i.e. one standard deviation from the ensemble mean). Nevertheless, an additional uncertainty may arise depending on whether the ice caps are further delineated into outlet glaciers or

considered as one entity as here. Also, the scaling relations for ice caps have not been validated in the same way as has been done for mountain glaciers (e.g. Radić et al. 2008; Adhikari and Marshall 2012).

4.4.2 Error propagation

In this section we attempt to provide a bulk error analysis due to propagation of errors assessed in model validation. We call this analysis bulk since the conventional error analysis cannot be applied here because it is impossible to verify whether all the necessary assumptions (normality, independence of parameters from each other, etc.) are satisfied. An alternative methodology to the conventional error analysis is to apply Monte-Carlo-like methods; however, since one run of our model takes several hours of computational time, we rule these methods out on computational grounds. In this analysis we assume that the RMSE of modeled in situ mass balance, assessed in model validation (Sect. 3.3), is the representative standard error (with an assumed 68 % confidence interval) for each glacier's specific mass balance in a given region. The results of the validation in terms of RMSE of annual mass balance for 14 regions are listed in Table 3. For the remaining five regions without the RMSE assessment we assume the following: Arctic Canada South has RMSE equal to the arithmetic mean of the RMSE of Arctic Canada North and Greenland (0.88 m w.e. year^{-1}), South Asia East and West have RMSE equal to that of Central Asia (1.05 m w.e. year^{-1}), the Low Latitudes region has RMSE equal to that of Southern Andes (1.48 m w.e. year^{-1}), while the Antarctic and Subantarctic region has RMSE equal to the arithmetic mean RMSE of all the other 18 regions (1.33 m w.e. year^{-1}). In this way, for each glacier in a given region we assign an error δ_B to its modeled specific mass balance, B (m w.e. year^{-1}). The regional volume change, expressed in SLE, for a given year is:

$$SLE(t) = -\frac{\sum_{i=1}^{N} B_i(t) S_i(t) \Delta t}{S_{ocean}} \quad (5)$$

where $B_i(t)$ is the modeled mass balance in specific units for a given glacier i, S_i is the glacier area, S_{ocean} is the area of the ocean (362×10^{12} m^2), N is the number of glaciers in the region, and $\Delta t = 1$ year. Assuming that the error of each glacier's area, δ_S, is 10 % of the glacier's area, S, we follow the principle of error propagation for a function of multiple variables (e.g. Bevington 1969) which gives the error, for a given year,

$$\delta_{SLE} = \sqrt{\sum_{i=1}^{N} \left(\frac{\partial SLE}{\partial B_i} \delta_{B_i} \right)^2 + \sum_{i=1}^{N} \left(\frac{\partial SLE}{\partial S_i} \delta_{S_i} \right)^2}. \quad (6)$$

Summing over all the 95 years (2006–2100) we find the cumulative error in the projected volume change by 2100. The results for each region are listed in Table 5. The Antarctic and Subantarctic is the region with the largest absolute error (5 mm SLE). In relative terms, New Zealand has the largest error (47 % for RCP4.5), followed by Alaska (26 %) and Antarctic and Subantarctic (25 %). The smallest relative errors are found in Russian Arctic (2 %), Svalbard (4 %) and Central Asia (4 %). On a global scale the error in projected SLE by 2100, forced by RCP4.5, is ±19 mm, which represents 12 % of the projected multi-model mean SLE. This error range is well below other assessed uncertainty ranges (±84 mm SLE from the sensitivity tests, ±41 mm SLE from the choice of GCM, 61 mm SLE as a difference between RCP8.5 and RCP4.5; Table 5).

4.4.3 Unquantified uncertainties

For detailed and extensive discussion about sources of uncertainty in projections of contributions from glaciers to sea-level rise we refer to Radić and Hock (2011). Here, as possible guidance for future work, we provide a brief summary of the uncertainties that are not yet quantified.

1. To our knowledge none of the current modeling studies of glacier volume changes incorporate mass loss by iceberg calving or submarine melt of marine-terminating glaciers. Studies on marine-terminating ice caps have shown that calving may account for roughly 30–40 % (e.g., Burgess et al. 2005; Dowdeswell et al. 2008) of total mass loss, a significant contribution if widely applicable. Gardner et al. (2013) estimate that the present day percentage of glacierized area draining into the ocean is ~35 %. However, calving estimates are scarce, and lacking on a global scale. Nevertheless, it may be expected that the fraction of total mass change due to calving will decrease as warming and terminus retreat proceed, and we assume that our projections of volume loss, in which only the loss due to the climatic mass balance is modeled, represent a lower bound.
2. Our mass balance model has many simplifications in order to make it usable on regional and global scales with few observations for model calibration and validation. The empirical parameters of the temperature-index model may not represent reality at the scale of individual glaciers. Also, the parameters and the transfer functions used to assess these parameters may not remain constant under future climate conditions.
3. Some studies have pointed out that variations in solar radiation can drive glacier mass changes (e.g. Huss et al. 2009). In regions such as our Low Latitudes region, where variations in radiation are the dominant driver of glacier mass changes, the performance of the

temperature-index model is limited. Hence, a better approach would be to apply a physically-based energy mass balance model, accounting for all components of the energy balance at the glacier surface. However, this remains a big challenge for models on regional and global scales that rely on projections from GCMs. Currently, the performance of GCMs in simulating surface radiation fluxes is insufficiently accurate for the purpose (Randall et al. 2007) and some form of GCM downscaling (dynamical or statistical) will introduce another spectrum of uncertainties.

4. Our representation of glacier dynamics using volume-area scaling remains a first-order approximation that is necessitated by the lack of input data (e.g. ice thickness) needed for physically-based ice dynamics models. However, as shown by Lüthi (2009), volume-area scaling has some serious shortcomings in modeling glacier volume evolution. The progress towards physically-based ice dynamics models that are fully coupled with mass balance models on regional scales is ongoing (Clarke et al. 2012), but challenging on a global scale.
5. Finally, we assume all glacier mass loss to contribute instantaneously, homogeneously, and directly to sea-level rise, and ocean area to remain constant. However, for more accurate estimates of the glacier contribution to sea-level rise one should correct for the glacier meltwater that flows into aquifers and enclosed basins rather than to the ocean, and also for isostatic adjustment of the land surface and the ocean floor to changes in ice and water loading, migration of grounding lines and shorelines, the presence of floating and grounded ice below sea level, and changes in ocean area. We note that, for the current projections, using sea-level equivalent is mainly a measure for how much water is lost from the glaciers, to allow for a simple interpretation and comparison with other contributions.

5 Conclusions

We have updated the projections of the glacier contribution to sea-level rise of Radić and Hock (2011) using a new global glacier inventory and two scenarios simulated by 14 GCMs prepared for IPCC AR5. Using the RCP4.5 emission scenario for 2006–2100 our multi-model mean (±1 standard deviation) suggests 155 ± 41 mm sea-level rise from glacier wastage by 2100, while the more extreme RCP8.5 emission scenario suggests higher sea-level rise of 216 ± 43 mm. These projections are higher than in Radić and Hock (2011) and IPCC AR4, which projected a range from 70 to 180 mm SLE for 2001–2100. Our results agree well with the projections of Marzeion et al. (2012) who found 166 ± 42 mm SLE (RCP4.5) and 217 ± 47 mm SLE (RCP8.5) using 15 GCMs.

The largest contributors to projected global volume loss are the glaciers in the Arctic (Canadian and Russian Arctic, Greenland, Alaska, Svalbard), contributing 104 ± 17 mm SLE by 2100 (RCP4.5), and glaciers in the Antarctic and Subantarctic contributing 21 ± 6 mm SLE. Arctic glaciers, though shown to be less sensitive to future temperature changes than the glaciers in mid and low latitudes, experience a pronounced amplification of temperature relative to lower latitudes in the GCM scenarios, with up to 5 K higher mean annual temperatures at the end of twenty-first century (2081–2100) relative to the mean over 2003–2022. The increase of the annual mean temperature in the Arctic is dominated by the warming in winter months, which results in reducing the range of the temperature seasonal cycle. The remaining regions, with a small fraction of present-day global ice volume, contribute 30 ± 9 mm SLE to global volume loss by 2100. However, some of these regions are projected to experience complete or almost complete deglaciation by the end of the century. For example Low Latitudes, Caucasus, Central Europe, Western Canada and US and Scandinavia are projected to lose more than 50 % of their current ice volume by 2050, and more than 80 % by 2100. This may have major implications for regional hydrology and water availability in the near future.

By using a new global glacier inventory our projections are free of the uncertainties due to upscaling an incomplete glacier inventory, the uncertainty that was unavoidable in the study of Radić and Hock (2011). Nevertheless, a large uncertainty range due to the choice of GCM and emission scenario remains. Additionally, our model calibration is highly sensitive to estimates of past and present regional mass changes which are used for model initialization. Uncertainty in those estimates may propagate an error as large as ± 84 mm SLE of global volume loss by 2100 for each GCM. To further narrow the uncertainty range of our projections we need to reduce the uncertainty in estimates of past and present global mass changes.

Acknowledgments Funding was provided by NASA grant (NNH10Z1A001N and NNX11AO23G) and NSF (grant EAR-0943742). We thank the two anonymous reviewers for their comments which helped us to significantly improve the manuscript.

References

Adhikari S, Marshall SJ (2012) Glacier volume-area relation for high-order mechanics and transient glacier states. Geophys Res Lett 39:L16505. doi:10.1029/2012GL052712

Arendt A et al (2012) Randolph glacier inventory: a dataset of global glacier outlines version: 2.0, 11 June 2012, GLIMS Technical Report

Bahr DB, Meier MF, Peckham SD (1997) The physical basis of glacier volume-area scaling. J Geophys Res 102(B9):20355–20362

Beck C, Grieser J, Rudolf B (2005) A new monthly precipitation climatology for the global land areas for the period 1951 to 2000. German Weather Service, Offenbach

Bevington PR (1969) Data reduction and error analysis for the physical sciences. McGraw-Hill, New York

Bliss A, Hock R, Cogley JG (2013) A new inventory of mountain glaciers and ice caps for the Antarctic periphery. Ann Glaciol 54(63):191–199. doi:10.3189/2013AoG63A377

Burgess D, Sharp M, Mair D, Dowdeswell J, Benham T (2005) Flow dynamics and iceberg calving rates of Devon Ice Cap, Nunavut, Canada. J Glaciol 51:219–230

Chen J, Ohmura A (1990) Estimation of Alpine glacier water resources and their change since the 1870's. Int Assoc Hydrol Sci Publ 193:127–135

Clarke GKC, Anslow FS, Jarosch AH, Radić V, Menounos B, Bolch T, Berthier E (2012) Ice volume and subglacial topography for western Canadian glaciers from mass balance fields, thinning rates, and a bed stress model. J Climate. doi:10.1175/JCLI-D-12-00513.1

Cogley JG (2009a) A more complete version of the World Glacier Inventory. Ann Glaciol 50(53):32–38

Cogley JG (2009b) Geodetic and direct mass-balance measurements: comparison and joint analysis. Ann Glaciol 50(50):96–100

Cogley JG et al (2011) Glossary of glacier mass balance and related terms. UNESCO-IHP

Columbus J, Sirguey P, Tenzer R (2011) A free, fully assessed 15-m DEM for New Zealand. Survey Q 66:16–19

de Woul M, Hock R (2005) Static mass balance sensitivity of Arctic glaciers and ice caps using a degree-day approach. Ann Glaciol 42:217–224

Dowdeswell JA, Benham TJ, Strozzi T, Hagen O (2008) Iceberg calving flux and mass balance of the Austfonna ice cap on Nordaustlandet, Svalbard. J Geophys Res 113:F03022

Dyurgerov MB (2010) Reanalysis of glacier changes: from the IGY to the IPY, 1960–2008. Data Glaciol Stud 108:1–116

Dyurgerov MB, Meier MF (2005) Glaciers and the changing earth system: a 2004 snapshot. INSTARR occasional paper 58, University of Colorado, Boulder

Gardner AS, Moholdt G, Cogley JG, Wouters B, Arendt AA, Wahr J, Berthier E, Hock R, Pfeffer WT, Kaser G, Ligtenberg SRM, Bolch T, Sharp MJ, Hagen JO, van den Broeke M, Paul F (2013) A consensus estimate of glacier contributions to sea level rise: 2003 to 2009. Science (accepted)

Hock R, de Woul M, Radić V, Dyurgerov M (2009) Mountain glaciers and ice caps around Antarctica make a large sea-level rise contribution. Geophys Res Lett 36:L07501. doi:10.1029/2008GL037020

Huss M (2011) Present and future contribution of glaciers to runoff from macroscale drainage basins in Europe. Water Resour Res 47:W07511. doi:10.1029/2010WR010299

Huss M, Funk M, Ohmura A (2009) Strong Alpine melt in the 1940s due to enhanced solar radiation. Geophys Res Lett 36:L23501

Huss M, Hock R, Bauder A, Funk M (2012) Conventional versus reference-surface mass balance. J Glaciol 58(208):278–286

Jarvis A, Reuter HI, Nelson A, Guevara E (2008) Hole-filled seamless SRTM data V4. http://srtm.csi.cgiar.org. Accessed 29 February 2012

Kållberg PW, Simmons AJ, Uppala SM, Fuentes M (2004) The ERA-40 Archive. ERA-40 Project Report Series 17, ECMWF, Reading

Kaser G, Cogley JG, Dyurgerov MB, Meier MF, Ohmura A (2006) Mass balance of glaciers and ice caps: consensus estimates for 1961–2004. Geophys Res Lett 33. doi:10.1029/2006GL027511

Kaser G, Großhauser M, Marzeion B (2010) Contribution potential of glaciers to water availability in different climate regimes. PNAS 107:20223–20227

Liu HK, Jezek K, Li B, Zhao Z (2001) Radarsat Antarctic mapping project digital elevation model version 2, Digital media. National Snow and Ice Data Center, Boulder. http://nsidc.org/data/nsidc-0082.html

Lüthi MP (2009) Transient response of idealized glaciers to climate change. J Glaciol 55(193):918–930

Marzeion B, Jarosch AH, Hofer M (2012) Past and future sea-level change from the surface mass balance of glaciers. Cryosphere 6:1295–1322. doi:10.5194/tc-6-1295-2012

Meier MF, Dyurgerov MB, Rick UK, O'Neel S, Pfeffer WT, Anderson RS, Anderson SP, Glazovsky AF (2007) Glaciers dominate eustatic sea-level rise in 21st century. Science 317:1064–1067

Moss RH (2010) The next generation of scenarios for climate change research and assessment. Nature 463:747–756. doi:10.1038/nature08823

Paul F, Haeberli W (2008) Spatial variability of glacier elevation changes in the Swiss Alps obtained from two digital elevation models. Geophys Res Lett 35:L21502

Radić V, Hock R (2006) Modelling mass balance and future evolution of glaciers using ERA-40 and climate models—A sensitivity study at Storglaciären, Sweden. J Geophys Res 111:F03003

Radić V, Hock R (2010) Regional and global volumes of glaciers derived from statistical upscaling of glacier inventory data. J Geophys Res 115:F01010. doi:10.1029/2009JF001373

Radić V, Hock R (2011) Regionally differentiated contribution of mountain glaciers and ice caps to future sea-level rise. Nat Geosci 4:91–94. doi:10.1038/NGEO1052

Radić V, Hock R, Oerlemans J (2007) Volume-area scaling vs flowline modelling in glacier volume projections. Ann Glaciol 46:234–240

Radić V, Hock R, Oerlemans J (2008) Analysis of scaling methods in deriving future volume evolutions of valley glaciers. J Glaciol 54(187):601–612

Randall DA et al (2007) Climate models and their evaluation. In: Solomon S et al (eds) IPCC climate change 2007: the physical science basis. Cambridge University Press, Cambridge

Raper SBC, Braithwaite RJ (2006) Low sea level rise projections from mountain glaciers and icecaps under global warming. Nature 439:311–313. doi:10.1038/nature04448

Rastner PN, Mölg T, Machguth H, Paul F (2012) The first complete glacier inventory for the whole of Greenland. Cryosphere 6:1483–1495. doi:10.5194/tc-6-1483-2012

Schiefer E, Menounos B, Wheate R (2007) Recent volume loss of British Columbia glaciers, Canada. Geophys Res Lett 34:L16503

Slangen ABA, Katsman CA, van de Wal RSW, Vermeersen LLA, Riva REM (2012) Towards regional projections of twenty-first century sea-level change based on IPCC SRES scenarios. Clim Dyn 38:1191–1209. doi:10.1007/s00382-011-1057-6

Tachikawa T, Hato M, Kaku M, Iwasaki A (2011) The characteristics of ASTER GDEM version 2, IGARSS

Taylor KE, Stouffer RJ, Meehl GA (2012) An overview of CMIP5 and the experiment design. Bull Am Meteorol Soc 93:485–498. doi:10.1175/BAMS-D-11-00094.1

Woodward J, Sharp M, Arendt A (1997) The influence of superimposed-ice formation on the sensitivity of glacier mass balance to climate change. Ann Glaciol 24:186–190

Zwally HJ, Schutz R, Bentley C, Bufton J, Herring T, Minster J, Spinhirne J, Thomas R (2012) GLAS/ICESat L2 Antarctic and Greenland Ice Sheet Altimetry Data V001. Boulder, CO: National Snow and Ice Data Center. Digital media